

Spatial curvature in $f(R)$ gravity

Christine R. Farrugia^{*} and Joseph Sultana[†]*Department of Mathematics, Faculty of Science, University of Malta, Msida MSD 2080, Malta*Jurgen Mifsud[‡]*Korea Astronomy and Space Science Institute, 776 Daedeokdae-ro, Yuseong-gu, Daejeon 34055, Republic of Korea**Institute of Space Sciences and Astronomy, University of Malta, Msida, MSD 2080, Malta*

(Received 8 June 2021; accepted 22 October 2021; published 1 December 2021)

In this work, we consider four $f(R)$ gravity models—the Hu-Sawicki, Starobinsky, Exponential and Tsujikawa models—and use a range of cosmological data, together with Markov Chain Monte Carlo sampling techniques, to constrain the associated model parameters. Our main aim is to compare the results we get when $\Omega_{k,0}$ is treated as a free parameter with their counterparts in a spatially flat scenario. The bounds we obtain for $\Omega_{k,0}$ in the former case are compatible with a flat geometry. It appears, however, that a higher value of the Hubble constant H_0 allows for more curvature. Indeed, upon including in our analysis a Gaussian likelihood constructed from the local measurement of H_0 , we find that the results favor an open universe at a little over 1σ . This is perhaps not statistically significant, but it underlines the important implications of the Hubble tension for the assumptions commonly made about spatial curvature. We note that the late-time deviation of the Hubble parameter from its Λ CDM equivalent is comparable across all four models, especially in the nonflat case. When $\Omega_{k,0} = 0$, the Hu-Sawicki model admits a smaller mean value for $\Omega_{\text{cdm},0}h^2$, which increases the said deviation at redshifts higher than unity. We also study the effect of a change in scale by evaluating the growth rate at two different wave numbers k_+ . Any changes are, on the whole, negligible, although a smaller k_+ does result in a slightly larger average value for the deviation parameter b .

DOI: [10.1103/PhysRevD.104.123503](https://doi.org/10.1103/PhysRevD.104.123503)

I. INTRODUCTION

Fourth-order metric theories of gravitation can be said to have originated from Weyl's 1918 nonintegrable relativity theory [1]. This theory (or variants of it) was further investigated by scientists such as W. Pauli, R. Weitzenböck and F. Jüttner, and served to introduce or promulgate key concepts such as conformal invariance, gravitational theories based on a geometrical approach, and the unification of the forces of Nature [2].¹ However, the popularity of Weyl's theory soon declined, namely due to the ambiguity of the associated Lagrangian and the problems posed by the higher order of the field equations. Additionally, there did not seem to be any experimental evidence against general relativity (GR) that would favor the introduction of a more complicated theory. It was not until the 1970s that interest was revived. This happened as a result of factors such as the one-loop renormalizability of fourth-order metric theories, and the natural way in which inflation can be incorporated into them [2].

Moreover, given a classical gravitational field arising from the energy-momentum tensor ($T_{\mu\nu}$) of quantized matter/radiation, the Lagrangian of fourth-order theories helps to erase any singularities that the gravitational interaction induces in $T_{\mu\nu}$ [3].

The general class of *fourth-order gravity* is governed by an action whose gravitational part reads [4,5]

$$\mathcal{S} = \int \frac{\sqrt{-g}}{16\pi G} f(R, R_{\alpha\beta}R^{\alpha\beta}, R_{\alpha\beta\gamma\delta}R^{\alpha\beta\gamma\delta}) d^4x, \quad (1)$$

where g is the determinant of the metric tensor $g_{\mu\nu}$, R , $R_{\alpha\beta}$ and $R_{\alpha\beta\gamma\delta}$ stand for the Ricci scalar and the Ricci and Riemann tensors, respectively, f represents a generic analytical function, and G is Newton's constant of gravitation. In the metric approach, the field equations are derived by varying the action with respect to $g^{\mu\nu}$ [5]. Among the theories obtained in this way is conformal Weyl gravity [6].

Another popular example is metric $f(R)$ gravity. Formulated by replacing the Ricci scalar in the GR action with a function thereof, $f(R)$ theory can be seen as a natural extension of GR [7]. Despite its simplicity, however, it incorporates some of the basic characteristics of higher-order

^{*}christine.r.farrugia@um.edu.mt[†]joseph.sultana@um.edu.mt[‡]jurgen.mifsud@um.edu.mt¹Also refer to works cited therein.

theories of gravity (i.e., theories constructed from actions in which the R of GR has been generalized to some function of higher-order curvature invariants), and is furthermore advantageous in that it appears to be the only higher-order theory that does not suffer from the Ostrogradski instability [8]. The prototype of $f(R)$ gravity has $f(R) = R - \alpha^4/R$ (where $\alpha \sim H_0$ and H_0 is the Hubble constant). It was adopted in an attempt to explain late-time cosmic acceleration [9–11], but has been ruled out on the basis of the Dolgov-Kawasaki instability [9,12] and the fact that it does not have a viable weak-field limit [9,13]. In general, the class of models with $f(R) = R + \alpha R^{-n}$ cannot give rise to an acceptable cosmological expansion history for any $n > 0$ or $n < -1$ [14].

The function associated with Starobinsky's inflationary model [$f(R) = R + \alpha R^2$] [15] was also one of the first to be proposed. Since then, $f(R)$ gravity has been the subject of numerous studies. One of its apparent benefits is the ability of certain models to reproduce both the early period of inflation and the current acceleration [16,17]. That said, due to the stringent constraints that a candidate model must satisfy—for example, it has to predict a matter-dominated cosmic era—only a few are still considered valid [7]. These are best tested on cosmological scales. Indeed, it is here that deviations from GR show up, so measurements of observables such as those related to galaxy clustering, the cosmic microwave background (CMB) or weak lensing are examples of pertinent cosmological probes [18].

Among the viable $f(R)$ models are the ones put forward by Hu and Sawicki [19], Starobinsky [20], Tsujikawa [21] and Cognola *et al.* [16]. The said models are the subject of numerous works in the literature (see, for instance, [7,22–30]), but almost always in the context of a spatially flat universe. In fact, the assumption that spatial curvature is negligible is made by the greater majority of works in the literature, with the results of missions such as *Planck* [31], WMAP [32], and SDSS [33] usually used as justification. The constraints placed by the respective studies on the geometry of the Universe are indeed compatible with spatial flatness. It should be remembered, however, that they are obtained in the context of a Λ CDM cosmology. And even with regards to the standard model, some issues remain: the *Planck* temperature (TT), polarization (EE+lowE) and temperature-polarization cross-correlation (TE) power spectra, for instance, appear to favor a closed universe² at over 2σ [31], but adding baryon acoustic oscillation (BAO) data or measurements of the full-shape galaxy power spectrum [FS- $P(k)$] makes the results perfectly consistent with a flat universe. The caveat is that the TT, TE, EE + lowE data turns out to be in significant tension with both BAO and FS- $P(k)$ measurements when a curved universe is assumed (see Ref. [34]

²Adding the lensing reconstruction reduces this to a little more than 1σ [31].

and works cited therein; using cosmic chronometers has been proposed as a solution [35]).

It is well-known that standard cosmic inflation predicts a flat geometry. This is because the curvature density parameter Ω_k decreases exponentially during the inflationary epoch, but only grows as a power law afterwards [36]. However, models of inflation that give rise to open [37,38] or closed universes [39,40] are also possible, although they often require a degree of fine tuning [36]. It has been suggested that spatial curvature could have emerged during the evolution of the Universe, once the growth of large-scale structure entered the nonlinear regime. This conclusion was reached on the basis of the silent Universe approximation [41]. The emergence of curvature might additionally hold the key to a resolution of the currently unresolved tension between CMB and distance-ladder estimates of the Hubble constant [42].

In view of this, the practice of setting $\Omega_{k,0}$ (the present-day value of Ω_k) to zero appears somewhat premature. There is also the fact that more stringent constraints on $\Omega_{k,0}$ could serve as important tests of eternal inflation models (see [43] and references therein). Furthermore, large-scale structure effects (such as those due to local inhomogeneities) could bias our measurements and shift the inferred $\Omega_{k,0}$ from the background value unless properly accounted for [43,44], as could higher-order perturbations like second-order lensing corrections [43]. Another point to keep in mind is the strong degeneracy that frequently exists between dark energy parameters and $\Omega_{k,0}$. Many times, the problem is circumvented either by setting the latter to zero, or by only considering specific classes of the former. A case in point is the dark energy equation-of-state (EoS) parameter, w_{de} , for which a functional form is usually assumed. The result is that spatial curvature is mostly studied in a rather restrictive framework. Of particular concern is the fact that if the true value of $\Omega_{k,0}$ deviates from zero, assuming a flat geometry induces errors in w_{de} that grow rapidly with redshift, even if the curvature is in reality only very small [45].

In this work, we consider four $f(R)$ models and use observational data to place bounds on cosmological and model-specific parameters. Our main aim is to investigate how constraints are affected if $\Omega_{k,0}$ is treated as a free parameter. First we go over the preliminary theory (Sec. II), then introduce the relevant likelihoods in Sec. III. Results are presented and discussed in Sec. IV, while Sec. V is dedicated to the concluding remarks. We use units in which the speed of light in vacuum, c , is equal to unity.

II. METRIC $f(R)$ GRAVITY: PRELIMINARIES

A. The field equations

At the basis of $f(R)$ theory is a generalization of the Einstein-Hilbert action of GR to:

$$\mathcal{S} = \int \frac{\sqrt{-g}}{16\pi G} f(R) d^4x. \quad (2)$$

Here, $f(R)$ is a generic function of the Ricci curvature scalar. The field equations are obtained by varying the action with respect to the inverse metric tensor $g^{\mu\nu}$ [9], and collectively read

$$\left(G_{\mu\nu} + \frac{1}{2}Rg_{\mu\nu} - \nabla_\mu\nabla_\nu + g_{\mu\nu}\square\right)f_R - \frac{1}{2}f(R)g_{\mu\nu} = 8\pi GT_{\mu\nu}, \quad (3)$$

where $G_{\mu\nu}$ is the Einstein tensor ($G_{\mu\nu} = R_{\mu\nu} - Rg_{\mu\nu}/2$), $f_R = df/dR$, the quantity ∇_μ represents the covariant derivative operator constructed from the metric connection, and $\square \equiv g_{\mu\nu}\nabla^\mu\nabla^\nu$. We shall model the matter/energy content of the Universe as a perfect fluid with proper density ρ , corresponding isotropic pressure p and four-velocity u^μ . The energy-momentum tensor of such a fluid reads

$$T_{\mu\nu} = (\rho + p)u_\mu u_\nu + pg_{\mu\nu}. \quad (4)$$

In a Friedmann-Lemaître-Robertson-Walker (FLRW) cosmology, the field equations [i.e., Eq. (3)] can be recast into the form of their general relativistic counterparts [22]. We may therefore write:

$$H^2 = \frac{8\pi G}{3}\rho_{\text{tot}} - \frac{\kappa}{a^2}, \quad (5)$$

$$\frac{\ddot{a}}{a} = -\frac{4\pi G}{3}(\rho_{\text{tot}} + 3p_{\text{tot}}). \quad (6)$$

In the above, a is the scale factor, normalized with respect to its present-day value, and $H = \dot{a}/a$ is the Hubble parameter; an overdot denotes differentiation with respect to cosmic time t . The parameter κ represents the spatial curvature and has dimensions of length^{-2} , while $\rho_{\text{tot}} = \rho + \rho_{\text{de}}$ and $p_{\text{tot}} = p + p_{\text{de}}$, ρ and p being the energy density and pressure from Eq. (4). However, while in GR ρ_{de} and p_{de} are attributes of a physical component—namely, the vacuum energy we denote by Λ —in $f(R)$ theory they may be expressed as a collection of terms which result from the modification to the geometry of the space-time manifold:

$$8\pi G\rho_{\text{de}} = \frac{1}{2}(f_R R - f) - 3H\dot{f}_R + 3(1 - f_R)H^2 + \frac{3\kappa}{a^2}(1 - f_R), \quad (7)$$

$$8\pi Gp_{\text{de}} = \frac{1}{2}(f - f_R R) + \ddot{f}_R - (1 - f_R)(2\dot{H} + 3H^2) + 2H\dot{f}_R + \frac{\kappa}{a^2}(f_R - 1). \quad (8)$$

Simply put, the impact of these geometric terms on cosmic dynamics mimics the effects of a dark energy component

with density ρ_{de} and pressure p_{de} [22]. We additionally note that this effective dark energy does not interact with matter or radiation. Consequently, conservation of energy implies that:

$$\dot{\rho} + 3H(\rho + p) = 0, \quad (9)$$

where $\rho = \rho_m$ (or ρ_r) and $p = p_m$ (or p_r). The subscripts “m” and “r” denote matter (cold dark matter and baryons) and radiation (photons and massless neutrinos), respectively.

As mentioned earlier, a valid $f(R)$ theory must fulfill a number of criteria [8,9,46,47]. First, since the quantity $G_{\text{eff}} \equiv G/f_R$ acts as an effective gravitational coupling, the requirement that the graviton carries positive kinetic energy implies that $G_{\text{eff}} > 0$, which in turn imposes the bound $f_R > 0$. Second, avoiding instabilities of the Dolgov-Kawasaki type [12] necessitates that $d^2f/dR^2 \geq 0$. As for the cosmological dynamics, the theory should behave like Λ CDM at high redshifts, because the standard model is well-supported by CMB data in this regime. We therefore expect that $\lim_{R \rightarrow \infty} f(R) = R + \text{constant}$. A late-time expansion history similar to the one in a Λ CDM cosmology is also desirable, albeit in the absence of a cosmological constant; that is to say, viable $f(R)$ models should satisfy the condition $\lim_{R \rightarrow 0} f(R) = R + 0$ [19].

The successes of Λ CDM on Solar System scales suggest that its phenomenology should be a limiting case [19] of any sound alternative theory. In metric $f(R)$, however, the Ricci curvature introduces a scalar degree of freedom, which could cause post-Newtonian constraints obtained from Solar System experiments to be violated. The model only remains valid if the scalar field can somehow be “shielded” from such experiments. This may be achieved via the so-called *chameleon mechanism*, whereby the effective mass M of the scalar varies according to the energy density of the local environment. In high-density regions like the Solar System, a large M would shorten the range of the scalar field to scales that cannot currently be probed by weak-field experiments. On the other hand, M would have to be small at cosmological densities, so as to allow the scalar field to act over a long range and drive the acceleration of the Universe [8,48,49]. One important thing to note about chameleon behavior is that it cannot be described as a fine-tuning mechanism. Rather, it is a natural and intrinsic property of those $f(R)$ models whose weak-field limit satisfies observational constraints.

Phase space analysis can also yield a wealth of information. In a particularly noteworthy study that takes this approach [14], the authors consider the quantities $m = [Rf_{RR}/f_R](r)$ (f_{RR} stands for d^2f/dR^2) and $r = -Rf_R/f$ and investigate the behavior of the $m(r)$ curve in the (r, m) plane. It is found that for an $f(R)$ model to admit a viable matter-dominated epoch, the curve should satisfy the conditions $m(r) \approx +0$ and $dm/dr > -1$ at $r \approx -1$. Additionally, a valid period of late-time

acceleration requires that $m = -r - 1$ while $(\sqrt{3} - 1)/2 < m \leq 1$ and $dm/dr < -1$, or that m lies in the range $(0, 1]$ at $r = -2$ [14].

B. The cosmological equations as a set of first-order differential equations

To avoid instabilities when solving Eqs. (5) and (6) numerically, we rewrite them as a set of first order ordinary differential equations. To this end, we follow Refs. [14,50–53]. The starting-point is the change of variables given by:

$$\begin{aligned} s &= \frac{R}{6(H_0^\Lambda \eta)^2}; & x &= -R'(z)(1+z); \\ y &= \frac{f(R)}{6f_R(H_0^\Lambda \eta)^2}; & \omega_m &= \frac{\Omega_{m,0}^\Lambda(1+z)^3}{\eta^2 f_R}; \\ \omega_r &= \frac{\Omega_{r,0}^\Lambda(1+z)^4}{\eta^2 f_R}; & K &= \frac{\kappa(1+z)^2}{(H_0^\Lambda \eta)^2}. \end{aligned} \quad (10)$$

Here, a prime denotes differentiation with respect to the argument and z is the cosmological redshift, while η is defined as the ratio H/H_0^Λ . $\Omega_{m,0}$ and $\Omega_{r,0}$ are the values of the matter and radiation density parameters at $z = 0$, respectively, and a superscript Λ indicates quantities as measured/inferred in the framework of a Λ CDM cosmology.

We have already seen that a candidate function $f(R)$ ideally satisfies the condition $\lim_{R \rightarrow \infty} f(R) = R + \text{constant}$. This implies that Eq. (2) becomes indistinguishable from the Einstein-Hilbert action at high redshifts, since the latter has Lagrangian density $(\sqrt{-g}/16\pi G)(R - 2\Lambda)$. Consequently, at early times the $f(R)$ cosmology behaves as a Λ CDM model having cosmological constant $\Lambda = -\text{constant}/2$. Let us reinterpret the superscript Λ as a label for the parameters of this specific Λ CDM model. If we write the quantity $-\text{constant}/2$ as $\Lambda^{f(R)}$, it follows that $\Lambda^\Lambda = \Lambda^{f(R)}$, and hence that

$$(H_0^\Lambda)^2 \Omega_{\Lambda,0}^\Lambda = (H_0^{f(R)})^2 \Omega_{\Lambda,0}^{f(R)}, \quad (11)$$

where $\Omega_{\Lambda,0}$ is the present-day value of the density parameter associated with Λ . Furthermore, given that the matter component is described by the same energy-momentum tensor in both Λ CDM and $f(R)$ gravity, and assuming that the two theories should lead to the same physical matter density today, we obtain the relation

$$\Omega_{m,0}^\Lambda (H_0^\Lambda)^2 = \Omega_{m,0}^{f(R)} (H_0^{f(R)})^2 = \frac{8\pi G}{3} \rho_m(z=0). \quad (12)$$

In general, though,

$$H_0^{f(R)} \neq H_0^\Lambda \quad \text{and} \quad \Omega_{m,0}^{f(R)} \neq \Omega_{m,0}^\Lambda. \quad (13)$$

since the two models are expected to diverge at late times [19,26].

A similar conclusion can be reached for the radiation density:

$$\Omega_{r,0}^\Lambda (H_0^\Lambda)^2 = \Omega_{r,0}^{f(R)} (H_0^{f(R)})^2; \quad \Omega_{r,0}^\Lambda \neq \Omega_{r,0}^{f(R)}. \quad (14)$$

In order to account for spatial curvature, it is customary to introduce a quantity $\Omega_{k,0}$ that complements $\Omega_{m,0}$ and $\Omega_{r,0}$ and is equal to $-\kappa/H_0^2$. The curvature parameter κ is a constant, so at early times an $f(R)$ model mimics a Λ CDM cosmology having $\kappa^\Lambda = \kappa^{f(R)}$. Therefore, it follows that

$$\Omega_{k,0}^\Lambda (H_0^\Lambda)^2 = \Omega_{k,0}^{f(R)} (H_0^{f(R)})^2. \quad (15)$$

κ is defined as the ratio k/\mathcal{R}_0^2 , k being the normalized curvature parameter (equal to ± 1 or 0) and \mathcal{R}_0 the present-day value of the non-normalized scale factor. So if $\kappa^\Lambda = \kappa^{f(R)}$, it must mean that at high redshifts, an $f(R)$ model with current scale factor $\hat{\mathcal{R}}_0$ behaves as a Λ CDM model that also has $\mathcal{R}_0 = \hat{\mathcal{R}}_0$.

Equations (12)–(15) make it possible to rewrite $H_0^{f(R)}$, $\Omega_{m,0}^{f(R)}$, $\Omega_{r,0}^{f(R)}$ and $\Omega_{k,0}^{f(R)}$ in terms of their Λ CDM counterparts [as was already done for the expressions in Eq. (10)]. This is especially convenient, because it enables us to construct informative priors for the $f(R)$ cosmological parameters using *Planck* constraints [31], which makes the process of sampling the parameter space much more efficient.

Let us now return to Eq. (10). In terms of the new variables (η , s , x , y , ω_m , ω_r , and K), the system of cosmological equations to be solved becomes:

$$\eta'(z) = \frac{\eta}{z+1} (2 - s + K); \quad (16)$$

$$s'(z) = -\frac{s}{z+1} \left(\frac{x}{R} + 4 - 2s + 2K \right); \quad (17)$$

$$\begin{aligned} x'(z) &= \frac{1}{\Gamma(z+1)} [(x\Gamma)^2 + s(x\Gamma - 1) + 3y - 1 + \omega_r \\ &\quad - K(1 + x\Gamma)] - x\Gamma'(z)\Gamma^{-1}; \end{aligned} \quad (18)$$

$$y'(z) = -\frac{1}{z+1} \left[s \frac{x}{R} + y(4 - x\Gamma - 2s + 2K) \right]; \quad (19)$$

$$\omega'_m(z) = \frac{\omega_m}{z+1} (x\Gamma + 2s - 2K - 1); \quad (20)$$

$$\omega'_r(z) = \frac{\omega_r}{z+1} (x\Gamma + 2s - 2K); \quad (21)$$

$$K'(z) = -\frac{2K}{z+1} (K - s + 1), \quad (22)$$

where Γ is equal to f_{RR}/f_R and serves to identify the particular $f(R)$ model.

C. Specific $f(R)$ models

Among the viable $f(R)$ models are the ones put forward by Hu and Sawicki [19], Starobinsky [20], Tsujikawa [21] and Cognola *et al.* [16]. In this subsection, we take a closer look at each of them in turn.

1. The Hu-Sawicki model

Hu and Sawicki proposed a class of “broken power-law” models [19]:

$$f(R)_{\text{HS}} = R - \mu^2 \frac{c_1 (R/\mu^2)^{n_{\text{HS}}}}{1 + c_2 (R/\mu^2)^{n_{\text{HS}}}}. \quad (23)$$

Here, c_1 and c_2 are dimensionless parameters, n_{HS} represents a positive constant that is usually assumed to be an integer, and $\mu^2 \approx \Omega_{m,0} H_0^2$.

It may be shown that the Hu-Sawicki model includes Λ CDM as a limiting case and can, in fact, be seen as a late-time modification of the latter [23]. Moreover, it is possible to explicitly incorporate the cosmological constant Λ into Eq. (23) by making the substitutions [30]

$$\Lambda = \frac{\mu^2 c_1}{2c_2}; \quad b = \frac{2c_2^{1-n_{\text{HS}}}}{c_1}, \quad (24)$$

which cast $f(R)_{\text{HS}}$ into the form [30,54]:

$$f(R)_{\text{HS}} = R - 2\Lambda \left(1 - \frac{1}{1 + [R/(b\Lambda)]^{n_{\text{HS}}}} \right). \quad (25)$$

Equation (25) makes it apparent that at high redshifts, when $R \gg \Lambda$, $f(R)_{\text{HS}}$ reduces to $R - 2\Lambda$ and Λ CDM is consequently recovered [54]. The differences that emerge at lower redshifts are quantified by the *deviation parameter* b [30] ($b = 0$ corresponds to Λ CDM). Constraints placed on b by means of cosmological data, therefore, translate into bounds on the allowed variation from the standard model. Additionally, the time at which these variations set in is controlled by n_{HS} : the larger the value of this parameter, the longer it takes for the Hu-Sawicki model to diverge from Λ CDM [19]. We shall follow other works in the literature and (without loss of generality) set n_{HS} to unity [22,23,30]. Furthermore, only non-negative values of b will be considered. The reason is that when $n_{\text{HS}} = 1$, $f_{RR} = 4b\Lambda^2/(R + b\Lambda)^3$, and so having $b < 0$ would mean that f_{RR} becomes negative as soon as $R > -b\Lambda$. We have already seen that viable $f(R)$ models have $f_{RR} \geq 0$.

Before proceeding to the next model, it would be interesting—and extremely useful for setting up the numerical procedures performed later—to determine at what redshift the Hu-Sawicki model becomes effectively

indistinguishable from Λ CDM. To this end, we adopt a procedure similar to the one proposed in Ref. [26] for exponential $f(R)$. Equation (25) allows us to deduce that if $f(R)_{\text{HS}}$ is to approach $R - 2\Lambda$ at high redshifts, the magnitude of $1/\{1 + [R^{f(R)}/(b\Lambda)]^{n_{\text{HS}}}\}$ must decrease asymptotically to zero as we go back in time. This may be expressed as the requirement that at some redshift z_{bound} , the quantity $1/(1 + [R^{f(R)}/(b\Lambda)]^{n_{\text{HS}}})$ is equal to ϵ (with $\epsilon \ll 1$), at which point any differences between the $f(R)$ model and Λ CDM are negligible. Moreover, at $z = z_{\text{bound}}$ one expects $R^{f(R)}$ to take the form $R^\Lambda + \xi$ (for some $|\xi| \ll R^\Lambda$). With these considerations in mind, we may write

$$\begin{aligned} 1 + \left(\frac{R^\Lambda + \xi}{b\Lambda} \right)^{n_{\text{HS}}} &\approx 1 + \left(\frac{R^{f(R)}}{b\Lambda} \right)^{n_{\text{HS}}} = \frac{1}{\epsilon}; \\ \Rightarrow \left(\frac{b\Lambda}{R^\Lambda + \xi} \right)^{n_{\text{HS}}} &\approx \frac{\epsilon}{1 - \epsilon}; \\ \Rightarrow \frac{b\Lambda}{R^\Lambda + \xi} &\approx \left(\frac{\epsilon}{1 - \epsilon} \right)^{n_{\text{HS}}^{-1}} = \nu; \\ \Rightarrow \frac{b\Lambda}{R^\Lambda} &\approx \nu \left(1 + \frac{\xi}{R^\Lambda} \right), \end{aligned}$$

and if terms higher than first order in ϵ or ξ/R^Λ are discarded, it follows that

$$\begin{aligned} \nu &= \left(\frac{\epsilon}{1 - \epsilon} \right)^{n_{\text{HS}}^{-1}} = e^{n_{\text{HS}}^{-1}} (1 - \epsilon)^{-n_{\text{HS}}^{-1}} \\ &\approx e^{n_{\text{HS}}^{-1}} \left(1 + \frac{\epsilon}{n_{\text{HS}}} \right) \approx e^{n_{\text{HS}}^{-1}}; \\ \frac{b\Lambda}{R^\Lambda} &\approx \nu \left(1 + \frac{\xi}{R^\Lambda} \right) \approx e^{n_{\text{HS}}^{-1}} \left(1 + \frac{\xi}{R^\Lambda} \right) \approx e^{n_{\text{HS}}^{-1}} \approx \nu. \quad (26) \end{aligned}$$

Therefore, $b\Lambda/R^\Lambda \approx \nu$ at $z = z_{\text{bound}}$. Using the relation $R^\Lambda = 3H_0^2[\Omega_{m,0}(1+z)^3 + 4\Omega_{\Lambda,0}]$, we solve for z_{bound} and find that

$$z_{\text{bound}} = \left[\frac{\Omega_{\Lambda,0}}{\Omega_{m,0}} \left(\frac{b}{\nu} - 4 \right) \right]^{1/3} - 1. \quad (27)$$

In the case of the Hu-Sawicki model, the ratio $b\Lambda/R^\Lambda$ (henceforth referred to as ν) equates to $[\epsilon/(1 - \epsilon)]^{n_{\text{HS}}^{-1}}$ at $z = z_{\text{bound}}$. The remaining models will give rise to different expressions for $b\Lambda/R^\Lambda$, which will all be functions of the quantity ϵ obtained by putting $f(R[z = z_{\text{bound}}]) = R - 2\Lambda(1 - \epsilon)$ (thus, ϵ differs from model to model). All we need to remember, however, is that ϵ is a positive constant much smaller than unity. More details about the values we choose for ϵ are given in Sec. III.

2. The Starobinsky model

Starobinsky proposed the function [20]:

$$f(R)_S = R + \lambda R_S \left[\left(1 + \frac{R^2}{R_S^2} \right)^{-n_S} - 1 \right], \quad (28)$$

where n_S and λ denote positive constants, and the third constant, R_S , is expected to be of the order of the present-day Ricci scalar [21]. We write $f(R)_S$ in the form of a perturbed Λ CDM Lagrangian [22]:

$$f(R)_S = R - 2\Lambda \left[1 - \left(1 + \frac{R^2}{(b\Lambda)^2} \right)^{-n_S} \right], \quad (29)$$

which clearly shows that $f(R)_S \rightarrow R - 2\Lambda$ when $R \gg \Lambda$ or when $b \rightarrow 0$. Λ and b may be expressed in terms of the original parameters as $\lambda R_S/2$ and $2/\lambda$, respectively [22].

The redshift z_{bound} is again given by Eq. (27). Now, however, we have that

$$\nu = \sqrt{\frac{e^{1/n_S}}{1 - e^{1/n_S}}}. \quad (30)$$

Without loss of generality, we shall put n_S equal to unity from now on.

3. The Exponential model

In this case, the $f(R)$ function reads [16]

$$f(R)_E = R + \beta [\exp(-\gamma R) - 1], \quad (31)$$

or equivalently [22]

$$f(R)_E = R - 2\Lambda \left[1 - \exp\left(-\frac{R}{b\Lambda}\right) \right], \quad (32)$$

with $\Lambda = \beta/2$ and $b = 2/(\gamma\beta)$. β and γ are two constants that characterize the model; γ must be positive so that $b \geq 0$ and at high redshifts, when $R \gg \Lambda$, the exponential function becomes negligible and Λ CDM is recovered [26]. This also happens as $b \rightarrow 0$.

The redshift z_{bound} may be estimated from Eq. (27) by making use of the relation

$$\nu = \frac{1}{\ln(1/\epsilon)}. \quad (33)$$

4. The Tsujikawa model

The model proposed by Tsujikawa is based on the function [21]

$$f(R)_T = R - \zeta R_T \tanh\left(\frac{R}{R_T}\right), \quad (34)$$

where ζ and R_T are positive constants. We may alternatively write

$$f(R)_T = R - 2\Lambda \tanh\left(\frac{R}{b\Lambda}\right). \quad (35)$$

Here, $b = 2/\zeta$ and $\Lambda = \zeta R_T/2$ [22], and the model becomes equivalent to Λ CDM either when $R \gg \Lambda$ or when $b \rightarrow 0$ (since $\tanh[R/(b\Lambda)] \rightarrow 1$ in both cases). The quantity ν required to calculate z_{bound} [Eq. (27)] is given by

$$\nu = \frac{1}{\text{arctanh}(1 - \epsilon)}. \quad (36)$$

D. Perturbations in $f(R)$ gravity

We start by considering the perturbed field equations:

$$\begin{aligned} \delta G_\nu^\mu f_R + (R_\nu^\mu - \nabla^\mu \nabla_\nu + \delta_\nu^\mu \square) f_{RR} \delta R + (\delta g^{\mu\alpha} \nabla_\nu \nabla_\alpha \\ - \delta_\nu^\mu \delta g^{\alpha\beta} \nabla_\alpha \nabla_\beta) f_R + (g^{\alpha\mu} \delta \Gamma_{\alpha\nu}^\gamma - \delta_\nu^\mu g^{\alpha\beta} \delta \Gamma_{\beta\alpha}^\gamma) \partial_\gamma f_R \\ = 8\pi G \delta T_\nu^\mu. \end{aligned} \quad (37)$$

In the above, the quantities δG_ν^μ , δR , $\delta g_{\mu\nu}$, and $\delta \Gamma_{\alpha\nu}^\mu$ denote perturbations in the Einstein tensor, the Ricci scalar, the metric tensor and the metric connection, respectively, while δ_ν^μ is the Kronecker delta. Perturbations in quantities related to the geometry of the space-time manifold appear on the left-hand side of Eq. (37). Meanwhile, the right-hand side constitutes the perturbed part δT_ν^μ of the energy-momentum tensor, and may be expanded as follows [55,56]:

$$\begin{aligned} \delta T_0^0 &= -\delta\rho_m; & \delta T_i^0 &= (\rho_m + p_m)v_i; \\ \delta T_0^i &= -(\rho_m + p_m)v^i; & \delta T_j^i &= \delta p_m \delta_j^i. \end{aligned} \quad (38)$$

Here, ρ_m and p_m are the background values of the matter energy density and pressure, respectively, and $\delta\rho_m$, δp_m their associated perturbations. The 3-vector v^i represents the perturbation in the spatial velocity. We keep to the perfect-fluid form and hence do not consider anisotropic stresses (which explains why $\delta T_j^i = 0$ for $i \neq j$) [57].

In the conformal Newtonian gauge, the perturbed FLRW metric takes the form:

$$ds^2 = a^2(\tau) [-(1 + 2\Phi)d\tau^2 + \gamma_{ij}(1 - 2\Psi)dx^i dx^j], \quad (39)$$

where $\gamma_{ij} = \delta_{ij} [1 + \frac{1}{4}\kappa(x^2 + y^2 + z^2)]^{-2}$ [57], τ is the conformal time (which is related to the cosmic time t via the scale factor: $d\tau = dt/a$), and we have made use of quasi-Cartesian coordinates [58].³ The scalar potentials $\Phi(\tau, \vec{x})$ and $\Psi(\tau, \vec{x})$ constitute the metric perturbations in

³In 3D Euclidean space with a Cartesian coordinate system, the 3-metric γ_{ij} has components δ_{ij} , rather than $\delta_{ij} [1 + \frac{1}{4}\kappa(x^2 + y^2 + z^2)]^{-2}$. We shall be using \vec{x} as shorthand for the spatial vector (x, y, z) .

our particular gauge; they are assumed to satisfy the condition $|\Phi|, |\Psi| \ll 1$.

The next step involves modeling perturbations as wave functions in momentum space. A perturbation $\delta g(\tau, \vec{x})$ in physical space translates into a sum (or integral) over k_{\dagger} -modes in momentum space. For instance, in the absence of spatial curvature, we have that

$$\delta g(\tau, \vec{x}) = \sum_{k_{\dagger}} \delta \hat{g}(\tau, k_{\dagger}) e^{i\vec{k}_{\dagger} \cdot \vec{x}}. \quad (40)$$

Each of the modes in question has a characteristic comoving wave vector \vec{k}_{\dagger} (and corresponding wave number $k_{\dagger} = |\vec{k}_{\dagger}|$). Since we consider perturbations to linear order only, it follows that if $\delta g(\tau, \vec{x})$ satisfies a particular equation, then the individual modes summed over in Eq. (40) also satisfy that equation, albeit for different values of k_{\dagger} . In other words, perturbations with a different wave number decouple, and so we can write our equations in terms of a generic mode $\delta \hat{g}(\tau, k_{\dagger}) Q(\vec{x}, k_{\dagger})$ [55,59]. In spherical coordinates, the purely spatial part of each mode of oscillation is given by

$$Q(\vec{x}, k_{\dagger}) = \Theta_{\beta(k_{\dagger})}^{\ell}(r) Y_{\ell m}(\theta, \phi), \quad (41)$$

where $Y_{\ell m}$ denotes the spherical harmonics and the form of the function Θ_{β}^{ℓ} depends on the value of κ (refer to [59,60] for more details). It may be shown that in the flat case, the right-hand side of Eq. (41) reduces to $e^{i\vec{k}_{\dagger} \cdot \vec{x}}$.

In momentum space, then, the time-time component of Eq. (37) reads [61]:

$$\begin{aligned} 2f_R \{ \Psi(k_{\dagger}^2 - 3\kappa) + 3\mathcal{H}[\Psi'(\tau) + \Phi\mathcal{H}] \} + f_{RR} [3\mathcal{H}'(\tau)\delta R \\ - k_{\dagger}^2 \delta R - 3\mathcal{H}\delta R'(\tau)] - 3\mathcal{H}\delta R f'_{RR}(\tau) + 3f'_R(\tau) [2\mathcal{H}\Phi \\ + \Psi'(\tau)] + 8\pi G a^2 \rho_m \delta_m = 0, \end{aligned} \quad (42)$$

with

$$\delta R = \frac{2}{a^2} \{ k_{\dagger}^2 (\Phi - 2\Psi) - 3[2\Phi\mathcal{H}'(\tau) + 3\mathcal{H}\Psi'(\tau) + \mathcal{H}\Phi'(\tau) \\ - 2\kappa\Psi + \Psi''(\tau) + 2\Phi\mathcal{H}^2] \}, \quad (43)$$

where \mathcal{H} is the conformal Hubble parameter [equivalent to the ratio $a'(\tau)/a$], and the matter density contrast function, δ_m , is defined as $\delta\rho_m/\rho_m$. We remark that, despite the hat notation $(\hat{\cdot})$ not being adopted, Φ , Ψ , δ_m and v actually correspond to $\hat{\Phi}(\tau, k_{\dagger})$, $\hat{\Psi}(\tau, k_{\dagger})$, $\hat{\delta}_m(\tau, k_{\dagger})$ and $\hat{v}(\tau, k_{\dagger})$, respectively; $Q(\vec{x}, k_{\dagger})$ has been factored out of Eqs. (42) and (43).

Contrary to what happens in Λ CDM, Φ and Ψ are not equal in $f(R)$ gravity [61]:

$$\Psi - \Phi = \frac{f_{RR}\delta R}{f_R}. \quad (44)$$

The above relation follows from the $i-j$ component ($i \neq j$) of Eq. (37). At this stage, we may simplify Eqs. (42) and (43) using the sub-Hubble and quasistatic approximations,⁴ whence they become:

$$2f_R \Psi(k_{\dagger}^2 - 3\kappa) - f_{RR} k_{\dagger}^2 \delta R + 8\pi G a^2 \rho_m \delta_m = 0; \quad (45)$$

$$\delta R = \frac{2}{a^2} [k_{\dagger}^2 (\Phi - 2\Psi) + 6\kappa\Psi]. \quad (46)$$

Let us now take a look at the perturbed version of energy-momentum conservation. The condition $\nabla_{\mu} T_{\nu}^{\mu} = 0$ still holds, but in this case $T_{\nu}^{\mu} = \tilde{T}_{\nu}^{\mu} + \delta T_{\nu}^{\mu}$ (the tilde denotes the unperturbed part), and the covariant derivative ∇_{μ} must be constructed from the perturbed metric tensor of Eq. (39) [65]. The relation $\nabla_{\mu} T_{\nu}^{\mu} = 0$ may consequently be expanded as follows:

$$\tilde{\nabla}_{\mu} \tilde{T}_{\nu}^{\mu} + \tilde{\nabla}_{\mu} \delta T_{\nu}^{\mu} + \delta \Gamma_{\sigma\mu}^{\mu} \tilde{T}_{\nu}^{\sigma} - \delta \Gamma_{\nu\mu}^{\sigma} \tilde{T}_{\sigma}^{\mu} = 0, \quad (47)$$

where $\tilde{\nabla}_{\mu}$ derives from the background metric, \tilde{T}_{ν}^{μ} is the unperturbed energy momentum tensor from Eq. (4), δT_{ν}^{μ} is its perturbed counterpart [Eq. (38)], and $\delta \Gamma_{\nu\sigma}^{\mu}$ represents the perturbed Christoffel symbols. The first term in Eq. (47) has no perturbed components and is therefore conserved separately, giving rise to the familiar relation⁵ $\rho'_m(\tau) = -3\mathcal{H}(\rho_m + p_m) = -3\mathcal{H}\rho_m(1 + w_m)$. The remaining terms yield the equations [61]:

$$\delta'_m(\tau) = (1 + w_m)[-k_{\dagger} v + 3\Psi'(\tau)]; \quad (48)$$

$$v'(\tau) = \mathcal{H}v(3w_m - 1) + k_{\dagger} \left(\Phi + \frac{w_m \delta_m}{1 + w_m} \right), \quad (49)$$

which can readily be combined to give:

$$\delta''_m(\tau) + \mathcal{H}\delta'_m(\tau) + k_{\dagger}^2 \Phi - 3\Psi''(\tau) - 3\mathcal{H}\Psi'(\tau) = 0, \quad (50)$$

provided that the matter component may be described as a distribution of dust (with $w_m = 0$). The parameter v that appears in Eqs. (48) and (49) is the velocity potential

⁴Sub-Hubble approximation: we assume that the relevant modes are well within the Hubble radius (the ‘‘horizon’’) during the time of interest, i.e., they have $k_{\dagger} \gg \mathcal{H}$.

Quasistatic approximation: can be stated as the condition that $|Y'(\tau)| \lesssim \mathcal{H}|Y|$, where $Y = \Phi, \Psi, \mathcal{H}, \Phi'(\tau), \Psi'(\tau)$ or $\mathcal{H}'(\tau)$ [62,63]. In other words, the temporal evolution of Y may essentially be attributed to the expansion of the Universe [64], and is thus negligible in comparison to any spatial changes (in Y).

⁵ w_m is the equation-of-state parameter for the matter component [not to be confused with ω_m from Eq. (10)].

associated with v^i . In momentum space, we have that⁶ $v_{\mathcal{S}}^i = -k_{\dagger}^{-1} \nabla_{*}^i v$, $\vec{\nabla}_{*}$ being the covariant derivative operator constructed from the (unperturbed) spatial metric γ_{ij} of Eq. (39). Under the sub-Hubble and quasistatic approximations, Eq. (50) further simplifies to

$$\delta_m''(\tau) + \mathcal{H}\delta_m'(\tau) + k_{\dagger}^2 \Phi = 0. \quad (51)$$

To obtain an expression for Φ , we insert Eq. (46) into Eqs. (44) and (45) and solve the last two for Φ (and Ψ), then use the solution to substitute for Φ in Eq. (51), which becomes [68]

$$\delta_m''(\tau) + \mathcal{H}\delta_m'(\tau) - 4\pi\rho_m\delta_m a^2 G_{\text{eff}} = 0, \quad (52)$$

with

$$\frac{G_{\text{eff}}}{G} = \frac{k_{\dagger}^2 [a^2 f_R + 4f_{RR}(k_{\dagger}^2 - 3\kappa)]}{f_R [3f_{RR}k_{\dagger}^2(k_{\dagger}^2 - 4\kappa) + a^2 f_R(k_{\dagger}^2 - 3\kappa)]}. \quad (53)$$

In terms of our new variables [see Eq. (10)], G_{eff}/G reads:

$$\frac{G_{\text{eff}}}{G} = \frac{k_{\dagger}^2 \omega_m a^3 \eta^2 [a^2 + 4\Gamma(k_{\dagger}^2 - 3\kappa)]}{\Omega_{m,0}^{\Lambda} [a^2(k_{\dagger}^2 - 3\kappa) + 3k_{\dagger}^2 \Gamma(k_{\dagger}^2 - 4\kappa)]}. \quad (54)$$

III. OBSERVATIONAL DATA AND CORRESPONDING LIKELIHOODS

In this section, we employ Bayesian statistics and place constraints on cosmological/model-specific parameters by utilizing Markov Chain Monte Carlo (MCMC) sampling techniques. We make use of a customized version of the Cosmic Linear Anisotropy Solving System (CLASS) v.2.6.3 [69], in conjunction with MONTE PYTHON v.3.0.1 [70,71]. For the MCMC part of the study, we consider as baseline parameters the quantities H_0 (in units of $\text{km s}^{-1} \text{Mpc}^{-1}$), $\Omega_{b,0} h^2$, $\Omega_{\text{cdm},0} h^2$, $\Omega_{k,0}$, b , n_s and $\ln(10^{10} A_s)$, where $\Omega_{b,0}$ and $\Omega_{\text{cdm},0}$ are the present-day values of the baryon and cold dark matter density parameters, respectively, n_s stands for the index of the primordial scalar power spectrum and A_s its amplitude, and h is equivalent to $H_0/(100 \text{ km s}^{-1} \text{Mpc}^{-1})$. The associated priors are listed in Table I. All other parameters take their CLASS default values, except for the reionization optical depth (which is set to 0.0544 [31]). A_s is varied subject to a Gaussian likelihood having a mean of 2.10×10^{-9} and a standard deviation of 0.03×10^{-9} [31].

⁶Every vector can be decomposed into the sum of a scalar part $v_{\mathcal{S}}^i$ (so called because it may be expressed as the gradient of a scalar field) and a vector part with zero divergence, $v_{\mathcal{V}}^i$ [57,66,67]. In first-order perturbation theory, the two parts evolve independently of each other, and only $v_{\mathcal{S}}^i$ contributes to the formation of structure [57].

TABLE I. The flat priors assigned to the baseline parameters.

Parameter	Min	Max
$H_0 (\text{km s}^{-1} \text{Mpc}^{-1})$	50	90
$\Omega_{b,0} h^2$	0.005	0.040
$\Omega_{\text{cdm},0} h^2$	0.05	0.20
$\Omega_{k,0}$	-0.3	0.3
b	0.0	1.0
n_s	0.75	1.25
$\ln(10^{10} A_s)$	2.8	3.2

The contour plots presented in this work were constructed using the MCMC analysis package GETDIST v.1.0.3 [72].

We compare model predictions with measurements of observables related to Type Ia supernovae (SNeIa), the cosmic microwave background (CMB), baryon acoustic oscillations (BAOs), cosmic chronometers and redshift-space distortions (RSDs). Below is a brief description of the respective datasets.

SNeIa: We make use of the Pantheon dataset, which is based on a sample of 1048 SNeIa in the redshift range $0.01 < z < 2.3$ [73].

CMB: Here, we work with four distance priors: the shift parameter \mathcal{R} , the acoustic scale l_A , the index of the primordial scalar power spectrum n_s , and the quantity $\Omega_{b,0} h^2$. The observational values of these four priors and the associated covariance matrix were obtained from Ref. [74].

BAO: Our dataset consists of the BAO measurements from the 6dF Galaxy Survey [75], as well as those derived from the main Galaxy sample of SDSS DR7 [76], the SDSS-DR12 Ly α -quasar cross-correlation function [77] and the Ly α -Forest catalogue from the same data release [78], and a BOSS galaxy selection constructed from the CMASS, LOWZ, LOWZE2 and LOWZE3 samples [79]. This choice of BAO data was made with the aim of removing or at least reducing potential correlations between BAO and RSD measurements.

Cosmic chronometers: The best cosmic chronometers are massive galaxies which acquired most of their stellar mass very rapidly at high redshifts, and have been evolving without major episodes of star formation since then. Consequently, their age may be inferred from that of their stellar population. Once the age difference Δt between two such galaxies (located at redshifts z and $z + \Delta z$) has been determined, it is possible to calculate $H(z)$ directly by means of the relation $H(z) = -(1+z)^{-1} \Delta z / \Delta t$ [80,81]. We consider the set of Hubble parameter values listed in Table II.

H_0^R : For part of the analysis, we make use of a Gaussian likelihood for H_0 constructed from the local measurement of Ref. [88], which was obtained via the distance-ladder approach and amounts to $74.03 \pm 1.42 \text{ km s}^{-1} \text{Mpc}^{-1}$.

TABLE II. Cosmic chronometer data. Each value of $H(z)$ is listed together with the corresponding redshift z and error σ .

Ref.	z	$H(z)$	σ
(km s ⁻¹ Mpc ⁻¹)			
[82]	0.0700	69.0	19.6
[82]	0.1200	68.6	26.2
[83]	0.1700	83.0	8.0
[81]	0.1791	75.0	4.0
[81]	0.1993	75.0	5.0
[82]	0.2000	72.9	29.6
[83]	0.2700	77.0	14.0
[82]	0.2800	88.8	36.6
[81]	0.3519	83.0	14.0
[84]	0.3802	83.0	13.6
[83]	0.4000	95.0	17.0
[84]	0.4004	77.0	10.2
[84]	0.4247	87.1	11.2
[84]	0.4497	92.8	12.9
[85] ^a	0.4700	89.0	49.6
[84]	0.4783	80.9	9.0
[86]	0.4800	97.0	62.0
[81]	0.5929	104.0	13.0
[81]	0.6797	92.0	8.0
[81]	0.7812	105.0	12.0
[81]	0.8754	125.0	17.0
[86]	0.8800	90.0	40.0
[83]	0.9000	117.0	23.0
[81]	1.0370	154.0	20.0
[83]	1.3000	168.0	17.0
[87]	1.3630	160.0	33.6
[83]	1.4300	177.0	18.0
[83]	1.5300	140.0	14.0
[83]	1.7500	202.0	40.0
[87]	1.9650	186.5	50.4

^aIn this case, σ was calculated by summing the systematic and statistical errors in quadrature.

The tension between this value of the Hubble constant and the *Planck* constraints on H_0 [31] is still unresolved, so it is crucial that we investigate any implications that an H_0 likelihood might have for the inferred $f(R)$ parameter constraints.

RSD: The collection of $f\sigma_8(z)$ data points we work with is provided in Table III, and has been adopted from the compilation in Ref. [89].

To calculate $f\sigma_8(z)$ for a given model, we need two quantities: the growth rate $f(z)$, and the standard deviation of density perturbations in spheres of radius $8h^{-1}$ Mpc, $\sigma_8(z)$. The former is a function of δ_m , the matter density contrast:

$$f = \frac{d(\ln \delta_m)}{d \ln a}. \quad (55)$$

 TABLE III. LSS data. Each $f\sigma_8(z)$ measurement is listed together with the corresponding redshift z and error $\sigma_{f\sigma_8}$, while Column 5 contains the values of $\Omega_{m,0}$ for the respective fiducial cosmologies.

Ref.	z	$f\sigma_8(z)$	$\sigma_{f\sigma_8}$	$\Omega_{m,0}^{\text{fid}}$
[90,91]	0.020	0.314	0.048	0.266
[92]	0.440	0.413	0.080	0.270
[92]	0.600	0.390	0.063	0.270
[92]	0.730	0.437	0.072	0.270
[93]	0.600	0.550	0.120	0.300
[93]	0.860	0.400	0.110	0.300
[94]	1.400	0.482	0.116	0.270
[95]	0.978	0.379	0.176	0.310
[95]	1.230	0.385	0.099	0.310
[95]	1.526	0.342	0.070	0.310
[95]	1.944	0.364	0.106	0.310

δ_m may in turn be obtained from Eq. (52) by solving it as part of the system of differential equations given by Eqs. (16)–(20) [with ω_r and K as defined in Eq. (10)].⁷

Since the expression for G_{eff}/G [Eq. (53)] is dependent on k_{\dagger} , it is necessary to choose an appropriate comoving wave number at which to evaluate $f(z)$. We shall focus exclusively on values of k_{\dagger} in the range $0.02h \text{ Mpc}^{-1} \leq k_{\dagger} \leq 0.2h \text{ Mpc}^{-1}$. This choice of bounds is based on two considerations: first, modes with $k_{\dagger} \lesssim 0.2h \text{ Mpc}^{-1}$ represent perturbations which may safely be considered linear [96], and second, the mode that crosses the horizon at matter-radiation equality has⁸ $k_{\dagger} \sim 0.015h \text{ Mpc}^{-1}$. The latter implies that smaller scales—corresponding to a larger k_{\dagger} —would be well within the horizon during the epochs of interest i.e., deep in the matter era and throughout the subsequent period of acceleration. We shall therefore determine $f(z)$ for two different values of k_{\dagger} : $k_{\dagger} = 0.1h \text{ Mpc}^{-1}$ and $k_{\dagger} = 0.05h \text{ Mpc}^{-1}$. In both cases, k_{\dagger}^2 is much larger than we could reasonably expect $|\kappa|$ to be ($k_{\dagger}^2 \gg |\kappa|$), and so Eq. (53) may be simplified to:

$$\frac{G_{\text{eff}}}{G} = \frac{a^2 f_R + 4f_{RR} k_{\dagger}^2}{f_R(3f_{RR} k_{\dagger}^2 + a^2 f_R)}. \quad (56)$$

Finally, to solve Eq. (52) we require a pair of initial conditions. The simplest choice is $\delta_m(a_{\text{ini}}) = a_{\text{ini}}$ and $\delta'_m(a = a_{\text{ini}}) = 1$ [or equivalently, $\delta_m(\tau_{\text{ini}}) = a_{\text{ini}}$ and $\delta'_m(\tau = \tau_{\text{ini}}) = H(a_{\text{ini}}) a_{\text{ini}}^2$], a_{ini} and τ_{ini} being the scale factor and conformal time, respectively, at which the initial

⁷We solve everything in terms of a by making use of the relations $d/dz = -a^2 d/da$ and $d/d\tau = Ha^2 d/da$.

⁸As calculated for a Λ CDM cosmology by using *Planck* values [31].

conditions are applied. However, this is only an option if two requirements are met: firstly, a_{ini} must correspond to a time when the Universe is deep in the matter-dominated epoch. Secondly, the given initial conditions are only valid for a Λ CDM cosmology [96]. This is where the quantity z_{bound} derived in Sec. II C turns out to be useful. Let us recall that when $z = z_{\text{bound}}$, $f(R) = R - 2\Lambda(1 - \epsilon)$ for some $\epsilon \ll 1$. Therefore, by calculating z_{bound} for a given set of values $\{b, \Omega_{m,0}, \Omega_{\Lambda,0}\}$, we can ensure that the initial conditions in question are applied during the “ Λ CDM epoch,” i.e., at a redshift $z_{\text{ini}} (= a_{\text{ini}}^{-1} - 1)$ which satisfies $z_{\text{ini}} \geq z_{\text{bound}}$. This is also important because z_{ini} is the redshift at which we stop providing the integrator with the equations for Λ CDM and switch to $f(R)$ [we check that the value of Γ exceeds machine precision before applying Eq. (18)].

Since we want z_{ini} to correspond to the matter-dominated epoch, the specific value of ϵ is dependent upon the dynamics of the model being considered. For instance, in the case of the Hu-Sawicki model, it suffices to have $\epsilon \sim 10^{-5}$. On the other hand, the Exponential model converges to Λ CDM extremely rapidly and hence a smaller ϵ ($\sim 10^{-50}$) works better.⁹ It should be noted, however, that the final results are *not* dependent on the exact value of ϵ (provided ϵ is sufficiently small). This was verified for both the Exponential and Tsujikawa models.

As previously suggested, the model is allowed to evolve identically to Λ CDM for redshifts $z > z_{\text{ini}}$. At $z = z_{\text{ini}}$, therefore, we must also specify initial conditions for Eqs. (16)–(20). These conditions are essentially the Λ CDM limits of η and the parameters defined in Eq. (10).

The second quantity we need in order to determine $f\sigma_8(z)$ is the standard deviation, $\sigma_8(z)$, which is given by:

$$\sigma_8^2(z) = \int_0^\infty \delta_m^2(z, k_\dagger) k_\dagger^{2+n_s} \left[\frac{4A_s k_*^{1-n_s}}{25H_0^4 \Omega_{m,0}^2} \right] T^2(k_\dagger) W^2(k_\dagger) dk_\dagger. \quad (57)$$

In the above, k_* denotes the pivot scale at which n_s and A_s are defined (here equal to 0.05 Mpc^{-1} [31]), and the function $W(k_\dagger)$ represents the Fourier transform of a spherical top-hat window function having radius R_8 ($= 8h^{-1} \text{ Mpc}$):

⁹In the case of the Exponential and Tsujikawa models, the convergence is so fast that δ_{ini} and δ'_{ini} must be applied at a redshift z_{ini} which is strictly greater than z_{bound} (if the condition of matter domination is to be met). To avoid computations with very small numbers, we switch from Λ CDM to $f(R)$ at a redshift z in the range $z_{\text{ini}} < z < z_{\text{bound}}$.

$$W(k_\dagger) = \frac{3}{k_\dagger^2 R_8^2} \left[\frac{\sin(k_\dagger R_8)}{k_\dagger R_8} - \cos(k_\dagger R_8) \right]. \quad (58)$$

We model the transfer function $T(k_\dagger)$ as detailed in the work of Eisenstein and Hu [97].

Since the density contrast function is not scale invariant in $f(R)$ gravity, every different value of k_\dagger we consider entails that we solve Eq. (52) numerically for δ_m over the required redshift range. The results are stored in a table, and at a given redshift z , $\delta_m(z, k_\dagger)$ is extracted from the table by interpolation for all relevant comoving wave numbers k_\dagger , and used to calculate the integrand in Eq. (57). Hence it becomes necessary to truncate the range of wave numbers over which integration is performed. To this end, we plot the integrand as a function of k_\dagger for various values of z , then infer the cutoff point from the outcome. Figure 1 shows a sample of such plots. The intuitive choice would be $k_\dagger \approx 0.5h \text{ Mpc}^{-1}$, but one must keep in mind that perturbations evolve nonlinearly for values of k_\dagger larger than around $0.2h \text{ Mpc}^{-1}$. Consequently, the linear perturbation equations we work with do not give an accurate description of structure growth beyond this limit. Nonetheless, $k_\dagger = 0.5h \text{ Mpc}^{-1}$ is a good starting point. We refine it further by calculating $\sigma_{8,0}$ [$= \sigma_8(z=0)$] for a Λ CDM cosmology from Eq. (57) and comparing it with the value returned by the default CLASS code. The two are closest when the upper integration limit is $\approx 0.4h \text{ Mpc}^{-1}$.

Finally, we correct for the Alcock-Paczynski effect by scaling (multiplying) the theoretical value of $f\sigma_8(z)$ by the

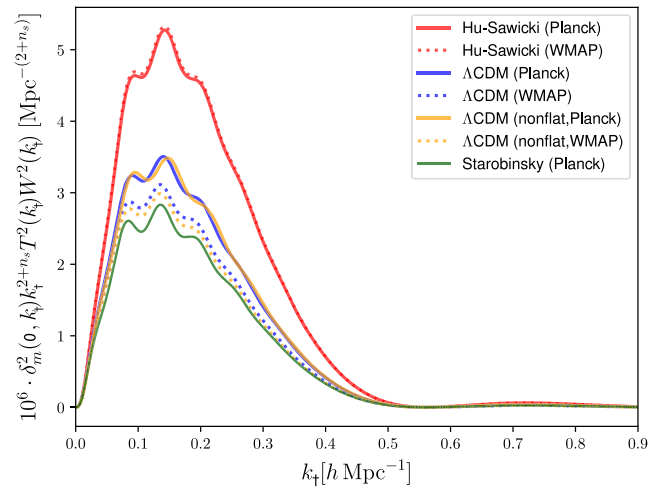


FIG. 1. The variation of the integrand in Eq. (57) with comoving wave number at $z = 0$ (only the k_\dagger -dependent part is plotted). The curves labeled “Hu-Sawicki” (“Starobinsky”) are based on the mean parameter values presented in Ref. [23] (Ref. [7]), with the remaining parameters fixed according to either the *Planck* 2018 [31] or the WMAP 9-year [32] results. The label “ Λ CDM” indicates that only *Planck* or WMAP values were used.

TABLE IV. Mean values and 1σ confidence intervals for the Hu-Sawicki model parameters.

Parameter	Flat	Nonflat	Nonflat ($+H_0^R$)	Nonflat
	$k_{\dagger} = 0.1h \text{ Mpc}^{-1}$	$k_{\dagger} = 0.1h \text{ Mpc}^{-1}$	$k_{\dagger} = 0.1h \text{ Mpc}^{-1}$	$k_{\dagger} = 0.05h \text{ Mpc}^{-1}$
H_0	$68.5280^{+0.4797}_{-0.4851}$	$68.6490^{+0.6385}_{-0.6645}$	$69.6890^{+0.6044}_{-0.6139}$	$68.6880^{+0.6543}_{-0.6640}$
$10^3 \Omega_{b,0} h^2$	$22.4790^{+0.1441}_{-0.1460}$	$22.4290^{+0.1727}_{-0.1714}$	$22.4500^{+0.1723}_{-0.1722}$	$22.4310^{+0.1776}_{-0.1808}$
$\Omega_{\text{cdm},0} h^2$	$0.1188^{+0.0010}_{-0.0010}$	$0.1195^{+0.0016}_{-0.0016}$	$0.1195^{+0.0015}_{-0.0016}$	$0.1194^{+0.0016}_{-0.0017}$
$10^3 \Omega_{k,0}$...	$0.8322^{+1.9912}_{-1.9341}$	$2.7676^{+1.8587}_{-1.8470}$	$0.8799^{+2.0596}_{-2.0515}$
$10^4 b$	$0.2739^{+0.1789}_{-0.2739}$	$0.7607^{+0.5798}_{-0.7607}$	$0.2089^{+0.0343}_{-0.2089}$	$1.9176^{+8.3473}_{-1.9176}$
n_s	$0.9705^{+0.0041}_{-0.0041}$	$0.9688^{+0.0051}_{-0.0051}$	$0.9689^{+0.0052}_{-0.0051}$	$0.9689^{+0.0054}_{-0.0053}$
$\ln(10^{10} A_s)$	$3.0442^{+0.0148}_{-0.0144}$	$3.0443^{+0.0148}_{-0.0145}$	$3.0442^{+0.0148}_{-0.0146}$	$3.0441^{+0.0148}_{-0.0145}$
$\Omega_{\Lambda,0}(\text{derived})$	$0.6989^{+0.0062}_{-0.0061}$	$0.6979^{+0.0062}_{-0.0062}$	$0.7049^{+0.0059}_{-0.0057}$	$0.6982^{+0.0067}_{-0.0065}$

factor $H_{\text{fid}}(z)d_{A,\text{fid}}(z)/H(z)d_A(z)$ [98,99], where $d_A(z)$ is the angular diameter distance to redshift z and a subscript ‘fid’ labels quantities pertaining to the fiducial cosmology. This refers to the cosmology in whose framework the *observational* value at the same redshift, $[f\sigma_8(z)]_{\text{obs}}$, was obtained.

IV. RESULTS

A. The Hu-Sawicki model

The mean values and 1σ confidence intervals for the Hu-Sawicki model are presented in Table IV, with a selection of 2D and 1D posterior distributions shown in Figs. 2 and 3. The tabulated results and the latter figure allow us to deduce that varying k_{\dagger} from $0.1h \text{ Mpc}^{-1}$ to $0.05h \text{ Mpc}^{-1}$ has minimal impact on the cosmological parameter constraints, but shifts the mean deviation parameter b to larger values. Another prominent characteristic is the negative correlation between $\Omega_{m,0}$ and H_0 . This is due to the fact that the theoretical expressions for many of the observables we use contain the product $\Omega_{m,0}H_0^2$, which implies that combinations of the parameters $\Omega_{m,0}$ and H_0 that give rise to the same value of $\Omega_{m,0}H_0^2$ are equally likely with respect to the observables in question. Similarly, the effects that variations in $\Omega_{k,0}$ would have on the primary CMB anisotropies may be offset by changes in H_0 . This happens if the angular diameter distance to last scattering remains unaltered [36], and explains the correlation between $\Omega_{k,0}$ and H_0 .

The addition of H_0^R to the dataset yields a larger mean value of H_0 , as expected. In view of the above-mentioned correlations, it becomes clear why this also causes a marked shift toward smaller (larger) values in the 1D posterior distribution for $\Omega_{m,0}$ ($\Omega_{k,0}$).

Fig. 2 illustrates how constraints are altered when the assumption of spatial flatness is relaxed. On the whole, confidence intervals tend to become wider,¹⁰ with the difference being most apparent for the $\Omega_{m,0}$ vs H_0 contour

plot. Indeed, the negative correlation between the two quantities is much stronger for a flat universe. This feature arises due to the fact that H_0 is correlated with $\Omega_{k,0}$.

B. The Starobinsky model

The inferred parameter constraints, including those for the deviation parameter, are presented in Table V and in Figs. 4 and 5. The effects that using a different wave number, introducing curvature or including a Gaussian likelihood for H_0 have on the constraints are much the same as for the Hu-Sawicki model. We again note that the mean value of b becomes slightly larger when $k_{\dagger} = 0.05h \text{ Mpc}^{-1}$ (relative to what we get when $k_{\dagger} = 0.1h \text{ Mpc}^{-1}$ in the nonflat case), and that the H_0^R likelihood makes the

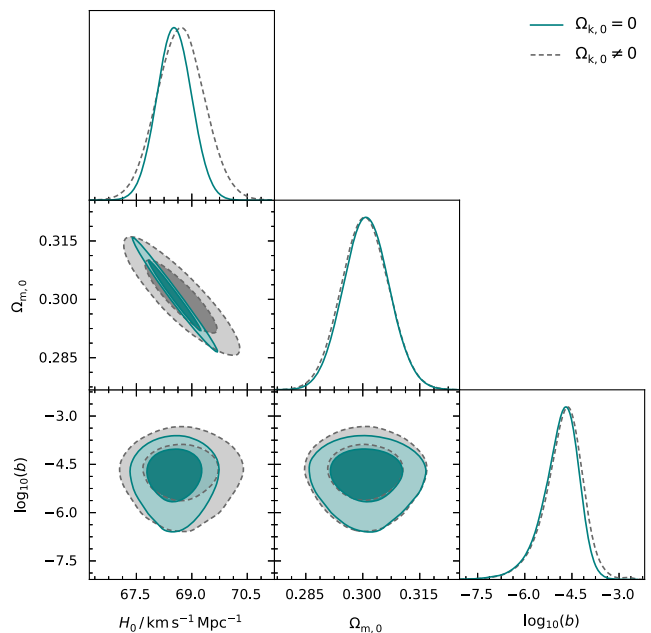


FIG. 2. A comparison between the posterior distributions for the main parameters of the spatially flat ($\Omega_{k,0} = 0$) Hu-Sawicki model and its nonflat ($\Omega_{k,0} \neq 0$) counterpart. Darker (lighter) shades denote 1σ (2σ) confidence regions.

¹⁰This is easier to deduce from the tabulated results.

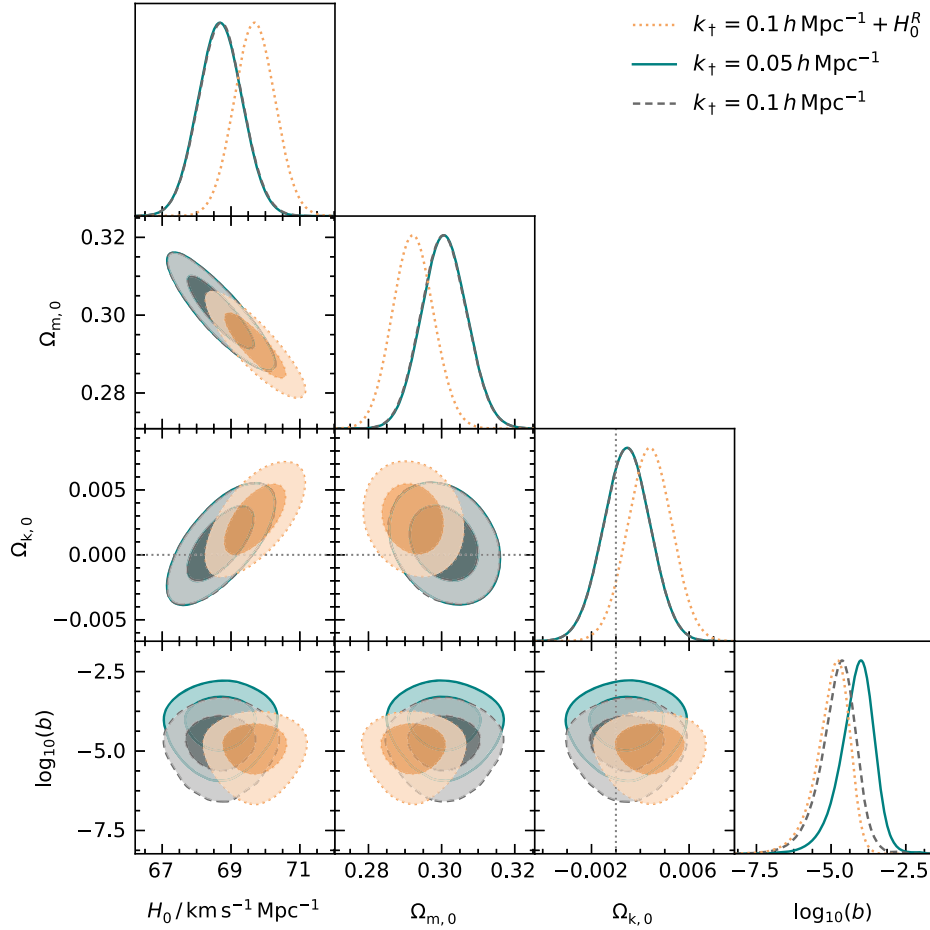


FIG. 3. Marginalized 2D and 1D posterior distributions for the main parameters of the spatially nonflat Hu-Sawicki model. The ‘+ H_0^R ’ that appears in the legend indicates the use of a Gaussian likelihood for H_0 .

TABLE V. Mean values and 1σ confidence intervals for the Starobinsky model parameters.

Parameter	Flat	Nonflat	Nonflat (+ H_0^R)	Nonflat
	$k_{\dagger} = 0.1 h \text{ Mpc}^{-1}$	$k_{\dagger} = 0.1 h \text{ Mpc}^{-1}$	$k_{\dagger} = 0.1 h \text{ Mpc}^{-1}$	$k_{\dagger} = 0.05 h \text{ Mpc}^{-1}$
H_0	$68.4080^{+0.4792}_{-0.4852}$	$68.6270^{+0.6541}_{-0.6569}$	$69.5520^{+0.6097}_{-0.6178}$	$68.5910^{+0.6512}_{-0.6586}$
$10^3 \Omega_{b,0} h^2$	$22.4560^{+0.1451}_{-0.1442}$	$22.4260^{+0.1700}_{-0.1734}$	$22.4390^{+0.1716}_{-0.1718}$	$22.4250^{+0.1703}_{-0.1729}$
$\Omega_{\text{cdm},0} h^2$	$0.1191^{+0.0010}_{-0.0010}$	$0.1195^{+0.0015}_{-0.0015}$	$0.1196^{+0.0015}_{-0.0016}$	$0.1195^{+0.0015}_{-0.0015}$
$10^3 \Omega_{k,0}$...	$0.8160^{+1.9832}_{-1.9055}$	$2.6443^{+1.8679}_{-1.8506}$	$0.7448^{+2.0605}_{-1.8984}$
b	$0.0122^{+0.0055}_{-0.0122}$	$0.0057^{+0.0011}_{-0.0057}$	$0.0064^{+0.0074}_{-0.0064}$	$0.0132^{+0.0021}_{-0.0132}$
n_s	$0.9699^{+0.0041}_{-0.0041}$	$0.9687^{+0.0051}_{-0.0051}$	$0.9686^{+0.0052}_{-0.0051}$	$0.9687^{+0.0050}_{-0.0051}$
$\ln(10^{10} A_s)$	$3.0441^{+0.0149}_{-0.0144}$	$3.0443^{+0.0149}_{-0.0143}$	$3.0442^{+0.0149}_{-0.0145}$	$3.0442^{+0.0152}_{-0.0144}$
$\Omega_{\Lambda,0}$ (derived)	$0.6974^{+0.0063}_{-0.0060}$	$0.6976^{+0.0063}_{-0.0061}$	$0.7036^{+0.0059}_{-0.0057}$	$0.6974^{+0.0064}_{-0.0058}$

constraints on $\Omega_{k,0}$ compatible with a spatially curved universe at $\sim 1\sigma$.

C. The Exponential model

Here, the mean values for the deviation parameter b are significantly larger than the ones obtained in the context of

the Hu-Sawicki and Starobinsky models. As may be inferred from Table VI, the constraints on b are consistent with zero, i.e., with the Λ CDM limit, within a 2σ confidence interval. Moreover, from Figs. 6 and 7 we observe that the posteriors for $\log_{10} b$ are non-Gaussian. Including the H_0^R likelihood again leads to non-null spatial curvature at a little over 1σ .

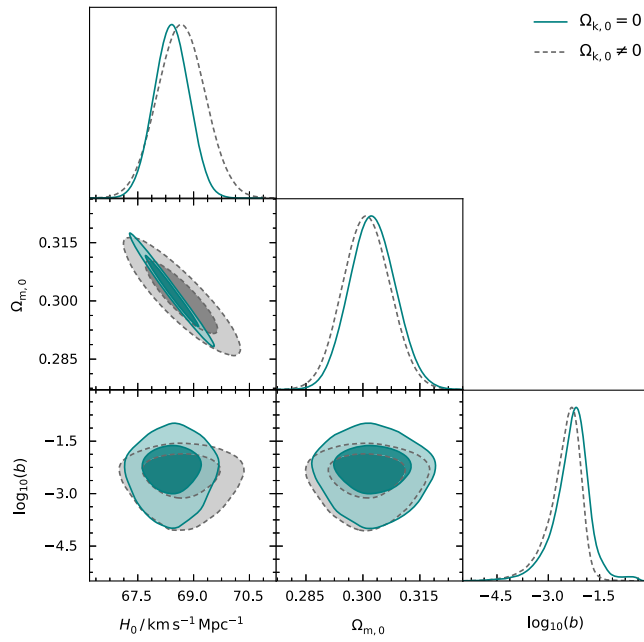


FIG. 4. A comparison between the posterior distributions for the main parameters of the spatially flat ($\Omega_{k,0} = 0$) Starobinsky model and its nonflat ($\Omega_{k,0} \neq 0$) counterpart.

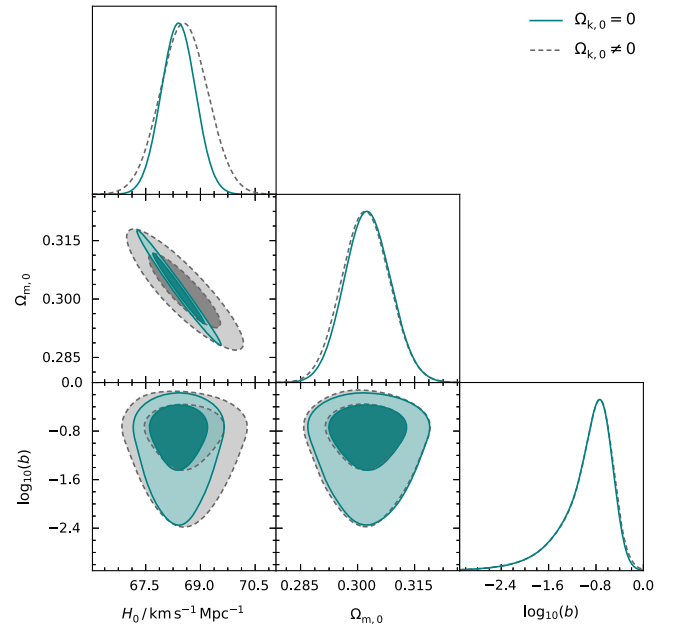


FIG. 6. A comparison between the posterior distributions for the main parameters of the spatially flat ($\Omega_{k,0} = 0$) Exponential model and its nonflat ($\Omega_{k,0} \neq 0$) counterpart.

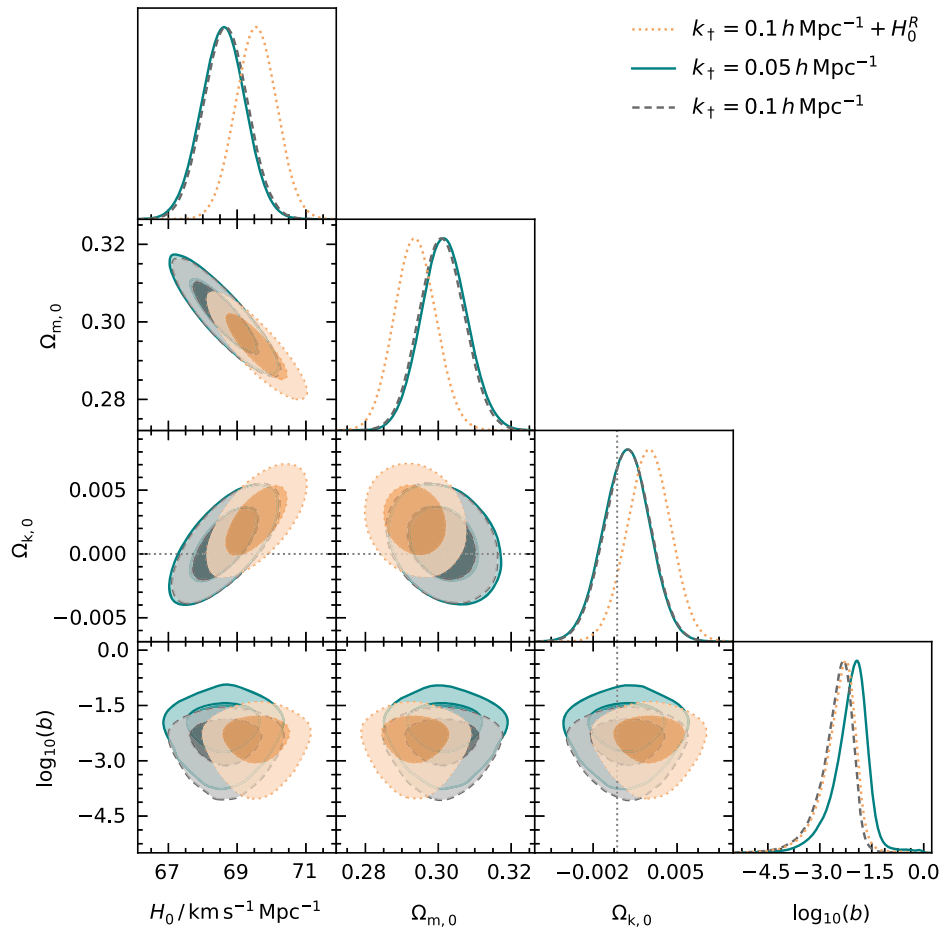


FIG. 5. Marginalized 2D and 1D posterior distributions for the main parameters of the spatially nonflat Starobinsky model.

TABLE VI. Mean values and 1σ confidence intervals for the Exponential model parameters.

Parameter	Flat	Nonflat	Nonflat ($+H_0^R$)	Nonflat
	$k_{\dagger} = 0.1h \text{ Mpc}^{-1}$	$k_{\dagger} = 0.1h \text{ Mpc}^{-1}$	$k_{\dagger} = 0.1h \text{ Mpc}^{-1}$	$k_{\dagger} = 0.05h \text{ Mpc}^{-1}$
H_0	$68.3990^{+0.4800}_{-0.4810}$	$68.5510^{+0.6598}_{-0.6648}$	$69.5060^{+0.6030}_{-0.6096}$	$68.5650^{+0.6520}_{-0.6657}$
$10^3\Omega_{b,0}h^2$	$22.4560^{+0.1457}_{-0.1448}$	$22.4210^{+0.1701}_{-0.1719}$	$22.4360^{+0.1702}_{-0.1697}$	$22.4220^{+0.1719}_{-0.1715}$
$\Omega_{\text{cdm},0}h^2$	$0.1191^{+0.0010}_{-0.0010}$	$0.1195^{+0.0016}_{-0.0016}$	$0.1196^{+0.0015}_{-0.0016}$	$0.1195^{+0.0015}_{-0.0016}$
$10^3\Omega_{k,0}$...	$0.7000^{+2.0506}_{-1.9734}$	$2.5938^{+1.8411}_{-1.8318}$	$0.7216^{+1.9878}_{-1.9544}$
b	$0.1601^{+0.0916}_{-0.1565}$	$0.1641^{+0.0850}_{-0.1599}$	$0.1608^{+0.1800}_{-0.1800}$	$0.1769^{+0.0920}_{-0.1727}$
n_s	$0.9697^{+0.0041}_{-0.0041}$	$0.9686^{+0.0051}_{-0.0052}$	$0.9684^{+0.0051}_{-0.0051}$	$0.9686^{+0.0051}_{-0.0052}$
$\ln(10^{10}A_s)$	$3.0443^{+0.0147}_{-0.0146}$	$3.0441^{+0.0149}_{-0.0144}$	$3.0440^{+0.0148}_{-0.0145}$	$3.0442^{+0.0149}_{-0.0144}$
$\Omega_{\Lambda,0}$ (derived)	$0.6972^{+0.0063}_{-0.0061}$	$0.6971^{+0.0063}_{-0.0061}$	$0.7032^{+0.0060}_{-0.0057}$	$0.6971^{+0.0063}_{-0.0061}$

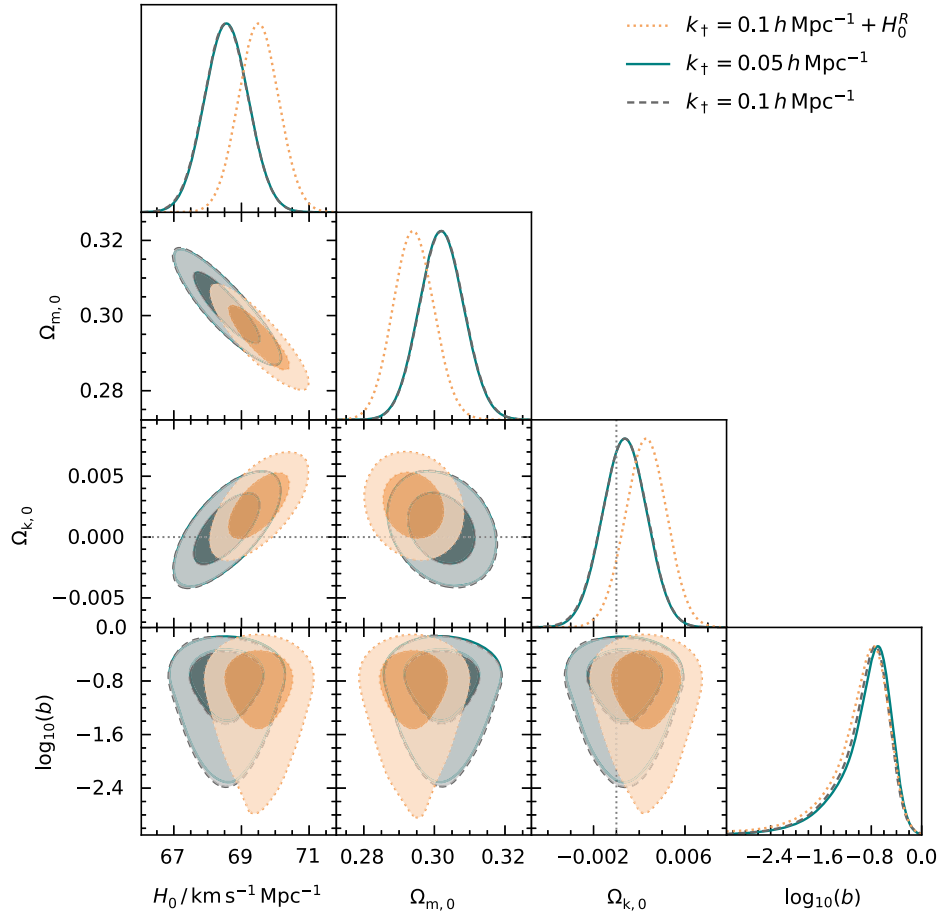


FIG. 7. Marginalized 2D and 1D posterior distributions for the main parameters of the spatially nonflat Exponential model.

D. The Tsujikawa model

The derived confidence regions for the main parameters of this model are depicted in Figs. 8 and 9, where we represent a selection of pairwise posterior probability functions. We also show the corresponding marginalized 1D distributions. In similar fashion to the Exponential model, the posterior distributions for $\log_{10} b$ are characterized

by a non-Gaussian profile, and the constraints on b include the Λ CDM limit, i.e., $b = 0$, within a 2σ confidence interval.

We report the inferred mean parameter values and the associated uncertainties in Table VII. As was observed for the other $f(R)$ models, $\Omega_{k,0}$ deviates from zero at a little over 1σ when we introduce a likelihood for H_0 .

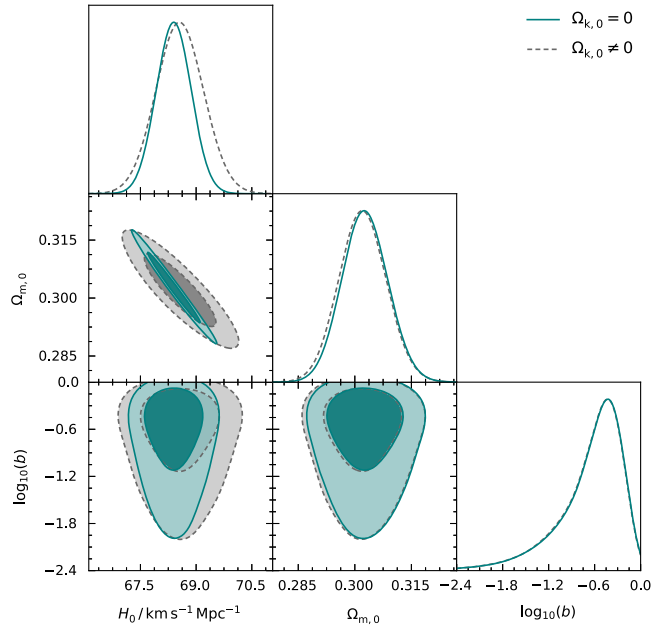


FIG. 8. A comparison between the posterior distributions for the main parameters of the spatially flat ($\Omega_{k,0} = 0$) Tsujikawa model and its nonflat ($\Omega_{k,0} \neq 0$) counterpart.

E. Comparison with Λ CDM

Next, we use the same datasets to constrain the parameters of the Λ CDM model, and consider three cases: (1) $\Omega_{k,0} = 0$, (2) freely varying $\Omega_{k,0}$, and (3) freely varying $\Omega_{k,0}$ plus a Gaussian likelihood for H_0 , with the latter constructed as outlined in Sec. III. The $f(R)$ models have an extra degree of freedom relative to Λ CDM (the deviation parameter, b). Hence, a robust comparison entails that we use a statistic which also takes this into account, because although more degrees of freedom can mean that the model is better able to approximate the data, this usually comes at the cost of weaker parameter constraints. We therefore employ the Akaike information criterion (AIC) [100]:

$$\text{AIC} = 2p - 2 \ln(\mathcal{L}_{\max}), \quad (59)$$

as well as the Bayesian information criterion (BIC) [101]:

$$\text{BIC} = p \ln N - 2 \ln(\mathcal{L}_{\max}), \quad (60)$$

and use them to gauge the performance of the $f(R)$ models in relation to Λ CDM. In the above equations, p is the amount of free parameters, N the number of

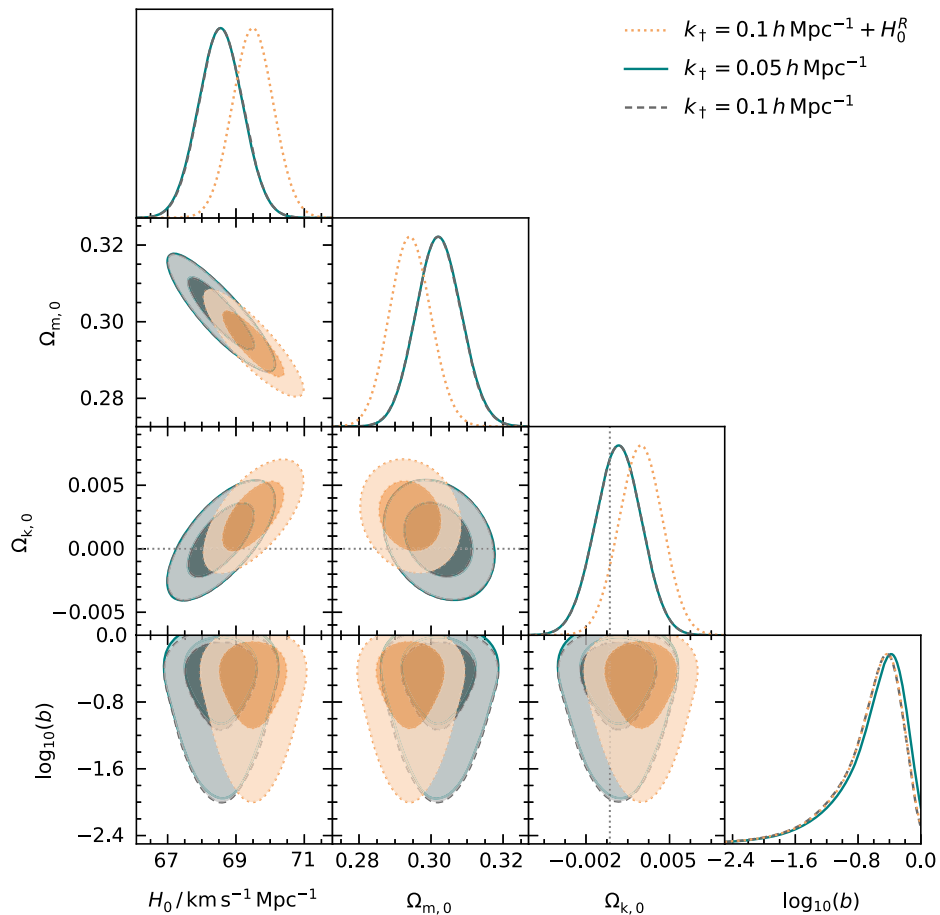


FIG. 9. Marginalized 2D and 1D posterior distributions for the main parameters of the spatially nonflat Tsujikawa model.

TABLE VII. Mean values and 1σ confidence intervals for the Tsujikawa model parameters.

Parameter	Flat	Nonflat	Nonflat ($+H_0^R$)	Nonflat
	$k_{\dagger} = 0.1h \text{ Mpc}^{-1}$	$k_{\dagger} = 0.1h \text{ Mpc}^{-1}$	$k_{\dagger} = 0.1h \text{ Mpc}^{-1}$	$k_{\dagger} = 0.05h \text{ Mpc}^{-1}$
H_0	$68.3970^{+0.4811}_{-0.4815}$	$68.5620^{+0.6480}_{-0.6591}$	$69.4970^{+0.6085}_{-0.6144}$	$68.5540^{+0.6552}_{-0.6608}$
$10^3 \Omega_{b,0} h^2$	$22.4550^{+0.1448}_{-0.1450}$	$22.4220^{+0.1713}_{-0.1712}$	$22.4340^{+0.1722}_{-0.1734}$	$22.4210^{+0.1706}_{-0.1706}$
$\Omega_{\text{cdm},0} h^2$	$0.1191^{+0.0010}_{-0.0010}$	$0.1195^{+0.0015}_{-0.0016}$	$0.1197^{+0.0016}_{-0.0016}$	$0.1196^{+0.0015}_{-0.0016}$
$10^3 \Omega_{k,0}$...	$0.7180^{+1.9853}_{-1.9563}$	$2.5897^{+1.8825}_{-1.8542}$	$0.7129^{+1.9839}_{-1.9624}$
b	$0.3028^{+0.1854}_{-0.2950}$	$0.2999^{+0.1775}_{-0.2920}$	$0.3022^{+0.1848}_{-0.2965}$	$0.3312^{+0.1815}_{-0.3235}$
n_s	$0.9697^{+0.0041}_{-0.0041}$	$0.9686^{+0.0052}_{-0.0051}$	$0.9684^{+0.0052}_{-0.0052}$	$0.9686^{+0.0051}_{-0.0051}$
$\ln(10^{10} A_s)$	$3.0443^{+0.0148}_{-0.0144}$	$3.0442^{+0.0149}_{-0.0145}$	$3.0442^{+0.0150}_{-0.0145}$	$3.0442^{+0.0149}_{-0.0145}$
$\Omega_{\Lambda,0}$ (<i>derived</i>)	$0.6972^{+0.0063}_{-0.0061}$	$0.6971^{+0.0063}_{-0.0061}$	$0.7031^{+0.0059}_{-0.0057}$	$0.6970^{+0.0063}_{-0.0061}$

TABLE VIII. The AIC and BIC statistics for the Hu-Sawicki, Starobinsky, Exponential, Tsujikawa and Λ CDM models. Δ AIC and Δ BIC are calculated by using the AIC and BIC values for Λ CDM as baseline. The constraints on the parameters of the standard model are independent of k_{\dagger} , so in this case we do not distinguish between the scenarios with $\Omega_{k,0} \neq 0$, $k_{\dagger} = 0.1h \text{ Mpc}^{-1}$ and $\Omega_{k,0} \neq 0$, $k_{\dagger} = 0.05h \text{ Mpc}^{-1}$.

Model	Statistic	Flat	Nonflat	Nonflat ($+H_0^R$)	Nonflat
		$k_{\dagger} = 0.1h \text{ Mpc}^{-1}$	$k_{\dagger} = 0.1h \text{ Mpc}^{-1}$	$k_{\dagger} = 0.1h \text{ Mpc}^{-1}$	$k_{\dagger} = 0.05h \text{ Mpc}^{-1}$
Hu-Sawicki	AIC	1089.02	1082.37	1106.86	1085.78
	Δ AIC	13.48	4.36	16.21	7.77
	BIC	1124.08	1122.43	1146.92	1125.84
	Δ BIC	18.50	9.37	21.21	12.78
Starobinsky	AIC	1077.55	1081.38	1093.36	1080.45
	Δ AIC	2.01	3.37	2.71	2.44
	BIC	1112.60	1121.44	1133.43	1120.51
	Δ BIC	7.02	8.38	7.72	7.45
Exponential	AIC	1077.13	1079.01	1092.32	1079.51
	Δ AIC	1.59	1.00	1.67	1.50
	BIC	1112.18	1119.07	1132.39	1119.57
	Δ BIC	6.60	6.01	6.68	6.51
Tsujikawa	AIC	1077.59	1079.66	1092.06	1079.51
	Δ AIC	2.05	1.65	1.41	1.50
	BIC	1112.64	1119.72	1132.13	1119.57
	Δ BIC	7.06	6.66	6.42	6.51
Λ CDM	AIC	1075.54	1078.01	1090.65	1078.01
	BIC	1105.58	1113.06	1125.71	1113.06

observations,¹¹ and \mathcal{L}_{max} denotes the maximum likelihood. When comparing two models, the quantity of interest is the difference between their AIC (BIC) values, as this indicates the level of support for the model with the smaller AIC (BIC): a $|\Delta\text{AIC}|$ that lies in the range from 2 to 4 provides considerable support, while values greater than 10 are effectively conclusive. In the case of the BIC, a difference of magnitude 2 is considered to favor the model having the smaller BIC, and (absolute) differences of 6 or more constitute strong evidence [102].

¹¹ $N = 1105$ in the absence of a likelihood for H_0 , and 1106 otherwise.

Our results are presented in Table VIII. The BIC penalizes more heavily for extra parameters, and in fact Λ CDM comes out on top when the five models are compared using this statistic. On the other hand, the AIC values for the Exponential and Tsujikawa models are relatively close to their Λ CDM counterparts, which implies that these $f(R)$ models perform similarly to Λ CDM when assessed with the AIC. The Starobinsky model is disfavored, albeit not strongly. The Hu-Sawicki model, however, appears to be ruled out by both information criteria. It is interesting to note that despite the extra free parameter, the nonflat models get lower AIC and BIC scores than the respective flat ones when no likelihood for H_0 has been included in the analysis.

The Starobinsky model is the only one that does not follow this trend.

The affinity of the Exponential and Tsujikawa models to Λ CDM concurs with the fact that for the greater majority of the cosmological evolution, they are essentially identical to the standard model. It is only at very late times that deviations set in, and when they do, they provide a neat mechanism for dark energy that is still painfully lacking in Λ CDM. These two models augment the benefits of Λ CDM with a well-motivated theoretical basis for the observed acceleration of the Universe, and in this sense are especially appealing.

V. CONCLUSION

The work presented here focuses on four $f(R)$ models and places constraints on their parameters by means of data from SNeIa, the CMB, BAOs, cosmic chronometers and RSDs.

The action of $f(R)$ gravity is constructed from that of GR by generalizing the Ricci scalar R to a function thereof. This results in a model that can be seen as a natural extension of GR, and that can furthermore explain the current accelerated expansion of the Universe without any need for dark energy. We study $f(R)$ gravity in the context of the Hu-Sawicki [19], Starobinsky [20], Exponential [16] and Tsujikawa [21] models. A common feature of these four models is the fact that the respective $f(R)$ functions can all be expressed in the form $f(R) = R - 2\Lambda X$, where Λ is the cosmological constant and X represents a quantity that goes to unity at high redshifts. Thus, any differences from Λ CDM emerge at late times.

The main aim of our work is to investigate in what ways, if any, the behavior of the models changes when the assumption of spatial flatness is relaxed. To this end, we use MCMC techniques to sample the parameter space of both cosmological and model-specific parameters, initially putting $\Omega_{k,0} = 0$, then allowing it to vary. As expected, constraints on cosmological parameters tend to be tighter when $\Omega_{k,0}$ is set to a fixed value. To further probe the role of curvature, we plot the ratio $H(z)/H_{\Lambda\text{CDM}}$ for each of the four models over the redshift range $[0, 5]$. $H(z)$ is evaluated by using the mean parameter values listed in Tables IV–VII, whereas $H_{\Lambda\text{CDM}}$ corresponds to a flat Λ CDM cosmology whose parameters are assigned the *Planck* values from Ref. [31]. Figure 10 shows that in the nonflat case (no H_0 likelihood), the departure from Λ CDM is comparable across the four models; any variations at low redshifts mainly arise from the fact that the models have a different Hubble constant. We have checked that this also holds if $k_{\dagger} = 0.05h \text{ Mpc}^{-1}$. Similar behavior is noted when we adopt the parameter values from the fourth column of Tables IV–VII, i.e., those obtained with an additional likelihood—a normal distribution constructed from the local measurement of H_0 . Now, however, the maximum value of $H(z)/H_{\Lambda\text{CDM}}$ increases, reflecting the higher averages we get for H_0

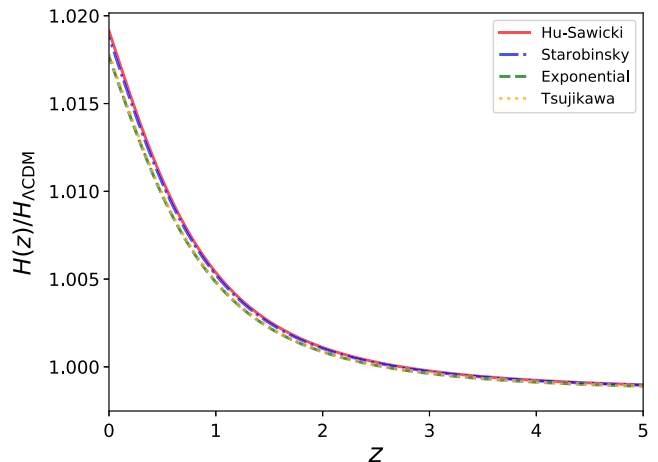


FIG. 10. The variation of $H(z)/H_{\Lambda\text{CDM}}$ with redshift at late times. $H(z)$ was calculated using the mean values from the third column of Tables IV–VII, and thus describes the expansion of a universe with $\Omega_{k,0} \neq 0$. $H_{\Lambda\text{CDM}}$ corresponds to a Λ CDM cosmology in which the density parameters and H_0 take the *Planck* TT, TE, EE + lowE + lensing mean values, and $\Omega_{k,0} = 0$. Therefore, the ratio $H(z)/H_{\Lambda\text{CDM}}$ does not go to unity at high redshifts.

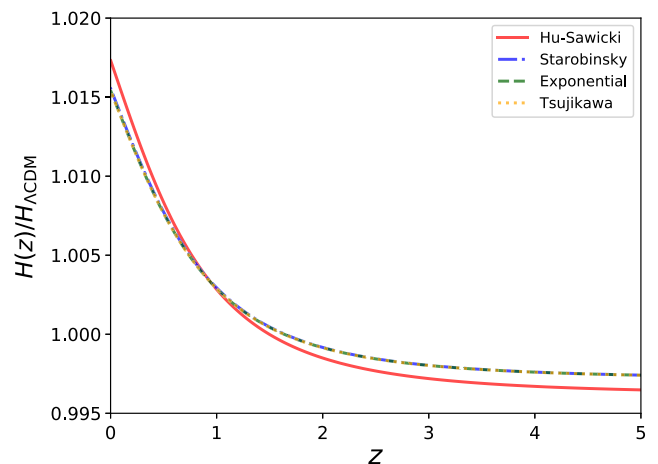


FIG. 11. Same as for Fig. 10, except that in this case, $H(z)$ is the Hubble parameter for a spatially flat universe, and was obtained using the mean values from the second column of Tables IV–VII.

in the presence of said likelihood. In the flat scenario, the curve for the Hu-Sawicki model stands out from the rest at redshifts $z > 1$ (Fig. 11). This is due to a larger deviation from Λ CDM, which may in turn be attributed to a smaller mean value of $\Omega_{\text{cdm},0}h^2$ (a quantity equal to 0.1188, compared to 0.1191 for the other models).¹²

¹²We point out that the separation between the Hu-Sawicki and the three other curves in Fig. 11 (for redshifts $z > 1$) is, in fact, not much bigger than that between the upper- and lower-most curves in some of the other cases we consider. The crucial difference is that here we do not get a gradual change from model to model.

On the whole, our results are consistent with spatial flatness. We note, nonetheless, that the constraints obtained upon adding H_0^R to the dataset favor an open universe at a little over 1σ . This is in line with the fact that H_0 is correlated with $\Omega_{k,0}$, so a higher mean value for the Hubble constant translates into a larger $\Omega_{k,0}$. It would seem prudent, therefore, not to exclude spatial curvature before the nature of the Hubble tension has been clarified. Indeed, model-independent estimates of $\Omega_{k,0}$, obtained in Ref. [103] using cosmic chronometer data and a Gaussian process reconstruction of the HII galaxy Hubble diagram, show that while the *Planck* value for the Hubble constant lends support to a flat universe, the local measurement of H_0 rules it out at around 3σ .

ACKNOWLEDGMENTS

J. M. would like to acknowledge funding support from Cosmology@MALTA (University of Malta) and KASI. The research work of C. F. disclosed in this publication was partially funded by the Endeavour Scholarship Scheme (Malta). Scholarships are part-financed by the European Union—European Social Fund (ESF)—Operational Programme II—Cohesion Policy 2014–2020: “*Investing in human capital to create more opportunities and promote the well-being of society*”. Numerical computations were carried out on the Sciama High Performance Compute (HPC) cluster, which is supported by the ICG, SEPNet and the University of Portsmouth.

-
- [1] H. Weyl, Gravitation und elektrizität, Sitzber. K. Preuss. Aka. **1918**, 465 (1918); Translated as ‘Gravitation and Electricity’, in *The Dawning of Gauge Theory*, L. O’Raifeartaigh (Princeton University Press, Princeton, New Jersey, 1997), pp. 24–37.
 - [2] H.-J. Schmidt, Fourth order gravity: Equations, history, and applications to cosmology, *Int. J. Geom. Methods Mod. Phys.* **04**, 209 (2007).
 - [3] R. Utiyama and B.S. DeWitt, Renormalization of a classical gravitational field interacting with quantized matter fields, *J. Math. Phys. (N.Y.)* **3**, 608 (1962).
 - [4] S. Capozziello and A. Stabile, The weak field limit of fourth order gravity, [arXiv:1009.3441v1](https://arxiv.org/abs/1009.3441v1).
 - [5] A. Stabile, Most general fourth-order theory of gravity at low energy, *Phys. Rev. D* **82**, 124026 (2010).
 - [6] P.D. Mannheim and D. Kazanas, Exact vacuum solution to conformal weyl gravity and galactic rotation curves, *Astrophys. J.* **342**, 635 (1989).
 - [7] J. Sultana, F. Melia, and D. Kazanas, Testing viable $f(R)$ models with the angular-diameter distance to compact quasar cores, *Phys. Rev. D* **99**, 103505 (2019).
 - [8] T. P. Sotiriou and V. Faraoni, $f(R)$ theories of gravity, *Rev. Mod. Phys.* **82**, 451 (2010).
 - [9] V. Faraoni, $f(R)$ gravity: Successes and challenges, [arXiv:0810.2602v1](https://arxiv.org/abs/0810.2602v1).
 - [10] S. Capozziello, S. Carloni, and A. Troisi, Quintessence without scalar fields, *Recent Res. Dev. Astron. Astrophys.* **1**, 625 (2003).
 - [11] S. M. Carroll, V. Duvvuri, M. Trodden, and M. S. Turner, Is cosmic speed-up due to new gravitational physics?, *Phys. Rev. D* **70**, 043528 (2004).
 - [12] A. Dolgov and M. Kawasaki, Can modified gravity explain accelerated cosmic expansion?, *Phys. Lett. B* **573**, 1 (2003).
 - [13] T. Chiba, $1/R$ gravity and scalar-tensor gravity, *Phys. Lett. B* **575**, 1 (2003).
 - [14] L. Amendola, R. Gannouji, D. Polarski, and S. Tsujikawa, Conditions for the cosmological viability of $f(R)$ dark energy models, *Phys. Rev. D* **75**, 083504 (2007).
 - [15] A. A. Starobinsky, A new type of isotropic cosmological models without singularity, *Phys. Lett. B* **91**, 99 (1980).
 - [16] G. Cognola, E. Elizalde, S. Nojiri, S.D. Odintsov, L. Sebastiani, and S. Zerbini, Class of viable modified $f(R)$ gravities describing inflation and the onset of accelerated expansion, *Phys. Rev. D* **77**, 046009 (2008).
 - [17] S. Nojiri and S.D. Odintsov, Modified gravity with negative and positive powers of curvature: Unification of inflation and cosmic acceleration, *Phys. Rev. D* **68**, 123512 (2003).
 - [18] A. De Felice and S. Tsujikawa, $f(R)$ Theories, *Living Rev. Relativity* **13**, 3 (2010).
 - [19] W. Hu and I. Sawicki, Models of $f(R)$ cosmic acceleration that evade solar system tests, *Phys. Rev. D* **76**, 064004 (2007).
 - [20] A. A. Starobinsky, Disappearing cosmological constant in $f(R)$ gravity, *J. Exp. Theor. Phys.* **86**, 157 (2007).
 - [21] S. Tsujikawa, Observational signatures of $f(R)$ dark energy models that satisfy cosmological and local gravity constraints, *Phys. Rev. D* **77**, 023507 (2008).
 - [22] R. C. Nunes, S. Pan, E. N. Saridakis, and E. M. C. Abreu, New observational constraints on $f(R)$ gravity from cosmic chronometers, *J. Cosmol. Astropart. Phys.* **01** (2017) 005.
 - [23] J. Pérez-Romero and S. Nesseris, Cosmological constraints and comparison of viable $f(R)$ models, *Phys. Rev. D* **97**, 023525 (2018).
 - [24] M. Martinelli, A. Melchiorri, and L. Amendola, Cosmological constraints on the Hu-Sawicki modified gravity scenario, *Phys. Rev. D* **79**, 123516 (2009).
 - [25] R. Arjona, W. Cardona, and S. Nesseris, Unraveling the effective fluid approach for $f(R)$ models in the subhorizon approximation, *Phys. Rev. D* **99**, 043516 (2019).

- [26] S. D. Odintsov, D. S.-C. Gómez, and G. S. Sharov, Is exponential gravity a viable description for the whole cosmological history?, *Eur. Phys. J. C* **77**, 862 (2017).
- [27] B. Hu, M. Raveri, M. Rizzato, and A. Silvestri, Testing Hu-Sawicki $f(R)$ gravity with the effective field theory approach, *Mon. Not. R. Astron. Soc.* **459**, 3880 (2016).
- [28] E. V. Linder, Exponential gravity, *Phys. Rev. D* **80**, 123528 (2009).
- [29] C.-Q. Geng, C.-C. Lee, and J.-L. Shen, Matter power spectra in viable $f(R)$ gravity models with massive neutrinos, *Phys. Lett. B* **740**, 285 (2015).
- [30] S. Basilakos, S. Nesseris, and L. Perivolaropoulos, Observational constraints on viable $f(R)$ parametrizations with geometrical and dynamical probes, *Phys. Rev. D* **87**, 123529 (2013).
- [31] N. Aghanim *et al.* (Planck Collaboration), Planck 2018 results. VI. Cosmological parameters, *Astron. Astrophys.* **641**, A6 (2020).
- [32] C. L. Bennett *et al.*, Nine-Year Wilkinson Microwave Anisotropy Probe (WMAP) observations: Final maps and results, *Astrophys. J. Suppl. Ser.* **208**, 20 (2013).
- [33] A. G. Sánchez, M. Crocce, A. Cabré, C. M. Baugh, and E. Gaztañaga, Cosmological parameter constraints from SDSS luminous red galaxies: A new treatment of large-scale clustering, *Mon. Not. R. Astron. Soc.* **400**, 1643 (2009).
- [34] S. Vagnozzi, E. Di Valentino, S. Gariazzo, A. Melchiorri, O. Mena, and J. Silk, The galaxy power spectrum take on spatial curvature and cosmic concordance, *Phys. Dark Universe* **33**, 100851 (2021).
- [35] S. Vagnozzi, A. Loeb, and M. Moresco, Eppur è piatto? The cosmic chronometers take on spatial curvature and cosmic concordance, *Astrophys. J.* **908**, 84 (2021).
- [36] P. A. R. Ade *et al.* (Planck Collaboration), Planck 2015 results: XIII. Cosmological parameters, *Astron. Astrophys.* **594**, A13 (2016).
- [37] M. Bucher, A. S. Goldhaber, and N. Turok, Open universe from inflation, *Phys. Rev. D* **52**, 3314 (1995).
- [38] A. Linde, Toy model for open inflation, *Phys. Rev. D* **59**, 023503 (1998).
- [39] A. Linde, Can we have inflation with $\Omega > 1$?, *J. Cosmol. Astropart. Phys.* **05** (2003) 002.
- [40] B. Ratra, Inflation in a closed Universe, *Phys. Rev. D* **96**, 103534 (2017).
- [41] K. Bolejko, Relativistic numerical cosmology with silent Universes, *Classical Quantum Gravity* **35**, 024003 (2018).
- [42] K. Bolejko, Emerging spatial curvature can resolve the tension between high-redshift CMB and low-redshift distance ladder measurements of the Hubble constant, *Phys. Rev. D* **97**, 103529 (2018).
- [43] C. D. Leonard, P. Bull, and R. Allison, Spatial curvature endgame: Reaching the limit of curvature determination, *Phys. Rev. D* **94**, 023502 (2016).
- [44] P. Bull and M. Kamionkowski, What if Planck's Universe isn't flat?, *Phys. Rev. D* **87**, 081301(R) (2013).
- [45] C. Clarkson, M. Cortês, and B. Bassett, Dynamical dark energy or simply cosmic curvature?, *J. Cosmol. Astropart. Phys.* **08** (2007) 011.
- [46] V. Faraoni, Matter instability in modified gravity, *Phys. Rev. D* **74**, 104017 (2006).
- [47] S. A. Appleby and R. A. Battye, Do consistent $F(R)$ models mimic general relativity plus Λ ?, *Phys. Lett. B* **654**, 7 (2007).
- [48] J. Khoury and A. Weltman, Chameleon Fields: Awaiting Surprises for Tests of Gravity in Space, *Phys. Rev. Lett.* **93**, 171104 (2004).
- [49] P. Brax, C. van de Bruck, A.-C. Davis, and D. J. Shaw, $f(R)$ gravity and chameleon theories, *Phys. Rev. D* **78**, 104021 (2008).
- [50] A. de la Cruz-Dombriz, P. K. S. Dunsby, S. Kandhai, and D. Sáez-Gómez, Theoretical and observational constraints of viable $f(R)$ theories of gravity, *Phys. Rev. D* **93**, 084016 (2016).
- [51] S. Carloni, A. Troisi, and P. K. S. Dunsby, Some remarks on the dynamical systems approach to fourth order gravity, *Gen. Relativ. Gravit.* **41**, 1757 (2009).
- [52] M. Abdelwahab, R. Goswami, and P. K. S. Dunsby, Cosmological dynamics of fourth-order gravity: A compact view, *Phys. Rev. D* **85**, 083511 (2012).
- [53] S. D. Odintsov and V. K. Oikonomou, Autonomous dynamical system approach for $f(R)$ gravity, *Phys. Rev. D* **96**, 104049 (2017).
- [54] K. Bamba, A. Lopez-Revelles, R. Myrzakulov, S. D. Odintsov, and L. Sebastiani, Cosmic history of viable exponential gravity: equation of state oscillations and growth index from inflation to dark energy era, *Classical Quantum Gravity* **30**, 015008 (2013).
- [55] J. M. Bardeen, Gauge-invariant cosmological perturbations, *Phys. Rev. D* **22**, 1882 (1980).
- [56] C.-P. Ma and E. Bertschinger, Cosmological perturbation theory in the synchronous and conformal newtonian gauges, *Astrophys. J.* **455**, 7 (1995).
- [57] V. F. Mukhanov, H. A. Feldman, and R. H. Brandenberger, Theory of cosmological perturbations, *Phys. Rep.* **215**, 203 (1992).
- [58] S. Weinberg, *Cosmology* (Oxford University Press, New York, 2008), pp. 2–5.
- [59] L. F. Abbott and R. K. Schaefer, A general, gauge-invariant analysis of the cosmic microwave anisotropy, *Astrophys. J.* **308**, 546 (1986).
- [60] E. R. Harrison, Normal modes of vibrations of the Universe, *Rev. Mod. Phys.* **39**, 862 (1967).
- [61] J.-C. Hwang and H. Noh, Gauge-ready formulation of the cosmological kinetic theory in generalized gravity theories, *Phys. Rev. D* **65**, 023512 (2001).
- [62] S. Tsujikawa, K. Uddin, and R. Tavakol, Density perturbations in $f(R)$ gravity theories in metric and Palatini formalisms, *Phys. Rev. D* **77**, 043007 (2008).
- [63] M.-C. Chiu, A. Taylor, S. Chenggang, and H. Tu, Cosmological perturbations and quasistatic assumption in $f(R)$ theories, *Phys. Rev. D* **92**, 103514 (2015).
- [64] G. Esposito-Farèse and D. Polarski, Scalar-tensor gravity in an accelerating Universe, *Phys. Rev. D* **63**, 063504 (2001).
- [65] A. de la Cruz-Dombriz, A. Dobado, and A. L. Maroto, Evolution of density perturbations in $f(R)$ theories of gravity, *Phys. Rev. D* **77**, 123515 (2008).

- [66] A. A. Asgari, A. H. Abbassi, and J. Khodagholizadeh, On the perturbation theory in spatially closed background, *Eur. Phys. J. C* **74**, 2917 (2014).
- [67] H. Kurki-Suonio, Cosmological perturbation theory, part 1, Lecture notes; University of Helsinki: Helsinki, Finland, 2020, www.courses.physics.helsinki.fi/teor/cpt/.
- [68] S. Tsujikawa, Matter density perturbations and effective gravitational constant in modified gravity models of dark energy, *Phys. Rev. D* **76**, 023514 (2007).
- [69] D. Blas, J. Lesgourgues, and T. Tram, The Cosmic Linear Anisotropy Solving System (CLASS). Part II: Approximation schemes, *J. Cosmol. Astropart. Phys.* **07** (2011) 034.
- [70] B. Audren, J. Lesgourgues, K. Benabed, and S. Prunet, Conservative constraints on early cosmology with MONTE PYTHON, *J. Cosmol. Astropart. Phys.* **02** (2013) 001.
- [71] T. Brinckmann and J. Lesgourgues, MontePython 3: Boosted MCMC sampler and other features, *Phys. Dark Universe* **24**, 100260 (2019).
- [72] A. Lewis, GetDist: A Python package for analysing Monte Carlo samples, [arXiv:1910.13970](https://arxiv.org/abs/1910.13970).
- [73] D. M. Scolnic *et al.*, The complete light-curve sample of spectroscopically confirmed SNe Ia from pan-STARRS1 and cosmological constraints from the combined Pantheon sample, *Astrophys. J.* **859**, 101 (2018).
- [74] Q.-G. Huang, K. Wang, and S. Wang, Distance priors from Planck 2015 data, *J. Cosmol. Astropart. Phys.* **12** (2015) 022.
- [75] F. Beutler, C. Blake, M. Colless, D. H. Jones, L. Staveley-Smith, L. Campbell, Q. Parker, W. Saunders, and F. Watson, The 6dF galaxy survey: Baryon acoustic oscillations and the local Hubble constant, *Mon. Not. R. Astron. Soc.* **416**, 3017 (2011).
- [76] A. J. Ross, L. Samushia, C. Howlett, W. J. Percival, A. Burden, and M. Manera, The clustering of the SDSS DR7 main Galaxy sample—I. A 4 per cent distance measure at $z = 0.15$, *Mon. Not. R. Astron. Soc.* **449**, 835 (2015).
- [77] H. du Mas des Bourboux *et al.*, Baryon acoustic oscillations from the complete SDSS-III Ly α -quasar cross-correlation function at $z = 2.4$, *Astron. Astrophys.* **608**, A130 (2017).
- [78] J. E. Bautista *et al.*, Measurement of baryon acoustic oscillation correlations at $z = 2.3$ with SDSS DR12 Ly α -Forests, *Astron. Astrophys.* **603**, A12 (2017).
- [79] S. Alam *et al.*, The clustering of galaxies in the completed SDSS-III Baryon Oscillation Spectroscopic Survey: Cosmological analysis of the DR12 galaxy sample, *Mon. Not. R. Astron. Soc.* **470**, 2617 (2017).
- [80] R. Jimenez and A. Loeb, Constraining cosmological parameters based on relative galaxy ages, *Astrophys. J.* **573**, 37 (2002).
- [81] M. Moresco *et al.*, Improved constraints on the expansion rate of the Universe up to $z \sim 1.1$ from the spectroscopic evolution of cosmic chronometers, *J. Cosmol. Astropart. Phys.* **08** (2012) 006.
- [82] C. Zhang, H. Zhang, S. Yuan, S. Liu, T.-J. Zhang, and Y.-C. Sun, Four new observational $H(z)$ data from luminous red galaxies in the Sloan Digital Sky Survey data release seven, *Res. Astron. Astrophys.* **14**, 1221 (2014).
- [83] J. Simon, L. Verde, and R. Jimenez, Constraints on the redshift dependence of the dark energy potential, *Phys. Rev. D* **71**, 123001 (2005).
- [84] M. Moresco, L. Pozzetti, A. Cimatti, R. Jimenez, C. Maraston, L. Verde, D. Thomas, A. Citro, R. Tojeiro, and D. Wilkinson, A 6% measurement of the Hubble parameter at $z \sim 0.45$: direct evidence of the epoch of cosmic re-acceleration, *J. Cosmol. Astropart. Phys.* **05** (2016) 014.
- [85] A. L. Ratsimbazafy, S. I. Loubser, S. M. Crawford, C. M. Cress, B. A. Bassett, R. C. Nichol, and P. Väisänen, Age-dating luminous red galaxies observed with the Southern African Large Telescope, *Mon. Not. R. Astron. Soc.* **467**, 3239 (2017).
- [86] D. Stern, R. Jimenez, L. Verde, M. Kamionkowski, and S. A. Stanford, Cosmic chronometers: Constraining the equation of state of dark energy. I: $H(z)$ measurements, *J. Cosmol. Astropart. Phys.* **02** (2010) 008.
- [87] M. Moresco, Raising the bar: New constraints on the Hubble parameter with cosmic chronometers at $z \sim 2$, *Mon. Not. R. Astron. Soc.: Lett.* **450**, L16 (2015).
- [88] A. G. Riess, S. Casertano, W. Yuan, L. M. Macri, and D. Scolnic, Large Magellanic Cloud cepheid standards provide a 1% foundation for the determination of the Hubble constant and stronger evidence for physics beyond Λ CDM, *Astrophys. J.* **876**, 85 (2019).
- [89] B. Sagredo, S. Nesseris, and D. Sapone, Internal robustness of growth rate data, *Phys. Rev. D* **98**, 083543 (2018).
- [90] T. Davis and B. Griffen, Cosmological constant, *Scholarpedia* **5**, 4473 (2010).
- [91] M. J. Hudson and S. J. Turnbull, The growth rate of cosmic structure from peculiar velocities at low and high redshifts, *Astrophys. J. Lett.* **751**, L30 (2012).
- [92] C. Blake *et al.*, The WiggleZ dark energy survey: Joint measurements of the expansion and growth history at $z < 1$, *Mon. Not. R. Astron. Soc.* **425**, 405 (2012).
- [93] A. Pezzotta *et al.*, The VIMOS Public Extragalactic Redshift Survey (VIPERS)—The growth of structure at $0.5 < z < 1.2$ from redshift-space distortions in the clustering of the PDR-2 final sample, *Astron. Astrophys.* **604**, A33 (2017).
- [94] T. Okumura *et al.*, The Subaru FMOS galaxy redshift survey (FastSound). IV. New constraint on gravity theory from redshift space distortions at $z \sim 1.4$, *Publ. Astron. Soc. Jpn.* **68**, 38 (2016).
- [95] G.-B. Zhao *et al.*, The clustering of the SDSS-IV extended Baryon Oscillation Spectroscopic Survey DR14 quasar sample: A tomographic measurement of cosmic structure growth and expansion rate based on optimal redshift weights, *Mon. Not. R. Astron. Soc.* **482**, 3497 (2019).
- [96] S. Dodelson, *Modern Cosmology* (Academic Press, San Diego, California, 2003), pp. 180–181.
- [97] D. J. Eisenstein and W. Hu, Baryonic features in the matter transfer function, *Astrophys. J.* **496**, 605 (1998).
- [98] E. Macaulay, I. K. Wehus, and H. K. Eriksen, Lower Growth Rate from Recent Redshift Space Distortion Measurements than Expected from Planck, *Phys. Rev. Lett.* **111**, 161301 (2013).
- [99] L. Kazantzidis and L. Perivolaropoulos, Evolution of the $f\sigma_8$ tension with the Planck15/ Λ CDM determination and

- implications for modified gravity theories, *Phys. Rev. D* **97**, 103503 (2018).
- [100] H. Akaike, A new look at the statistical model identification, *IEEE Trans. Autom. Control* **19**, 716 (1974).
- [101] G. Schwarz, Estimating the dimension of a model, *Ann. Stat.* **6**, 461 (1978).
- [102] S. Nesseris, A. De Felice, and S. Tsujikawa, Observational constraints on galileon cosmology, *Phys. Rev. D* **82**, 124054 (2010).
- [103] C.-Z. Ruan, F. Melia, Y. Chen, and T.-J. Zhang, Using spatial curvature with HII galaxies and cosmic chronometers to explore the tension in H_0 , *Astrophys. J.* **881**, 137 (2019).